SCIENCE AND TECHNOLOGY ORGANIZATION
CENTRE FOR MARITIME RESEARCH AND EXPERIMENTATION

Reprint Series **CMRE-PR-2019-072**

Physical and dynamical characteristics of a 300 m-deep anticyclonic eddy in the Ligurian Sea (Northwest Mediterranean Sea): evidence from a multi-platform sampling strategy

Ines Borrione, Silvia Falchetti, Alberto Alvarez

June 2019

Originally published in:

Deep Sea Research Part I: Oceanographic Research Papers, Elsevier, volume 116, October 2016, pp. 145-164, doi: https://doi.org/10.1016/j.dsr.2016.07.013

About CMRE

The Centre for Maritime Research and Experimentation (CMRE) is a world-class NATO scientific research and experimentation facility located in La Spezia, Italy.

The CMRE was established by the North Atlantic Council on 1 July 2012 as part of the NATO Science & Technology Organization. The CMRE and its predecessors have served NATO for over 50 years as the SACLANT Anti-Submarine Warfare Centre, SACLANT Undersea Research Centre, NATO Undersea Research Centre (NURC) and now as part of the Science & Technology Organization.

CMRE conducts state-of-the-art scientific research and experimentation ranging from concept development to prototype demonstration in an operational environment and has produced leaders in ocean science, modelling and simulation, acoustics and other disciplines, as well as producing critical results and understanding that have been built into the operational concepts of NATO and the nations.

CMRE conducts hands-on scientific and engineering research for the direct benefit of its NATO Customers. It operates two research vessels that enable science and technology solutions to be explored and exploited at sea. The largest of these vessels, the NRV Alliance, is a global class vessel that is acoustically extremely quiet.

CMRE is a leading example of enabling nations to work more effectively and efficiently together by prioritizing national needs, focusing on research and technology challenges, both in and out of the maritime environment, through the collective Power of its world-class scientists, engineers, and specialized laboratories in collaboration with the many partners in and out of the scientific domain.

NOTE: The CMRE Reprint series reprints papers and articles published by CMRE authors in the open literature as an effort to widely disseminate CMRE products. Users are encouraged to cite the original article where possible.

Contents lists available at ScienceDirect

Deep-Sea Research I

journal homepage: www.elsevier.com/locate/dsri

Physical and dynamical characteristics of a 300 m-deep anticyclonic eddy in the Ligurian Sea (Northwest Mediterranean Sea): Evidence from a multi-platform sampling strategy

Ines Borrione *, Silvia Falchetti, Alberto Alvarez [1]

NATO Science and Technology Organization, Centre for Maritime Research and Experimentation, Viale San Bartolomeo 400, 19126 La Spezia, Italy

ARTICLE INFO

Article history:
Received 18 November 2015
Received in revised form
27 July 2016
Accepted 28 July 2016
Available online 4 August 2016

Keywords:
Ligurian Sea
Mesoscale circulation
Anticyclonic eddy
Regional Ocean Modeling System
Gliders

ABSTRACT

We describe the physical and dynamical characteristics of a mesoscale anticyclonic eddy observed in August 2013 over the shelf-break region of the northeastern sector of the Ligurian Sea, between the northeastern edge of the Northern Current (NC) and the coast. Results derive from a dense dataset of temperature, salinity and current measurements obtained from a multi-platform sampling strategy as well as from a diagnostic simulation with the Regional Ocean Modeling System (ROMS) at a horizontal resolution of 1.8 km. Model results are obtained from a strong nudging to observations and, as they are physically balanced, they allow a three-dimensional diagnosis of the dynamics and physical characteristics of the eddy. The eddy is centered around 9.5°E, 43.94°N, about 20 km from the coast, and has a radius of 16 km. It is characterized by low-density waters and penetrates the thermocline down to at least 300 m reflecting the main features of the NC. Horizontal velocities near the surface are around 0.4 m s^{-1}, while at 150 m are still significantly high and close to 0.2 m s^{-1}. Vertical velocities were estimated from model results; absolute values are below 4 m day^{-1} until depths shallower than 150 m and increase with depth to 15 m day^{-1}. The eddy's presence inverts the northwestwards flow traditionally portrayed in the region determining a southeastwards coastal circulation that replenishes coastal waters with those originating from the NC. We discuss several possible eddy formation mechanisms and suggest that its formation depends on the directionality of the NC when it enters the Ligurian Sea, as a result of the adjustment of the shear and orbital components of the current's relative vorticity.

1. Introduction

The Ligurian-Provençal Basin (LPB) is located in the northwestern sector of the Mediterranean Sea, with the French-Italian border to its north, and Corsica Island to its south (Fig. 1). The eastern sector of the LPB is characterized by a wide continental shelf, which deepens gradually to maximum depths of 1000 m. Conversely, west of 9.5°E the continental shelf is narrower and the shelf slope is steep, reaching south of Genoa depths close to 2500 m. The rugged topography of the LPB plays an important role in guiding the main circulation pathways in the region (Millot et al., 1999; Taupier-Letage and Millot, 1986).

The main large scale hydrographic feature of the LPB is the Northern Current (NC), also known as the Liguro- Provençal -Catalan current (Millot et al., 1991). The NC forms to the north of Corsica Island as a result of the joining of the two currents flowing on either side of Corsica, i.e., the Western Corsica Current (WCC), and the Eastern Corsica Current (ECC), although several studies suggest that the NC is mainly driven by the ECC (Astraldi et al., 1990; Astraldi and Gasparini, 1992). The NC flows northwards north of Corsica and then southwestwards along the continental slope (Millot et al., 1999; Taupier-Letage and Millot, 1986), approximately 20–35 km offshore, along the Italian (west of Genoa) and French coast (Petrenko, 2003; Sammari et al., 1995; Schroeder et al., 2011), ending along the coast of Spain, where it enters the Catalan Sea (Birol et al., 2010; Millot et al., 1991). The result of the large scale circulation pattern in the LPB, composed of the northwards flowing WCC and the NC, is a deep cyclonic gyre (Millot, 1987, 1999).

A significant dynamical variability is superimposed onto the large scale circulation patterns described above. Several authors have documented the meandering nature of the NC (Crépon et al., 1982; Marullo et al., 1985), as well as the presence of eddy activity north of Corsica where the ECC converges with the WCC (Casella et al., 2014; Millot et al., 1991; Poulain et al., 2012; Sammari et al., 1995). Significant eddy activity has also been observed in other locations of the Northwest Mediterranean Sea like in the Gulf of

* Corresponding author.
E-mail address: Ines.Borrione@cmre.nato.int (I. Borrione).
[1] Present address: IMEDEA, Carrer Miquel Marquès 21, 07190 Esporles, Spain.

http://dx.doi.org/10.1016/j.dsr.2016.07.013
0967-0637/

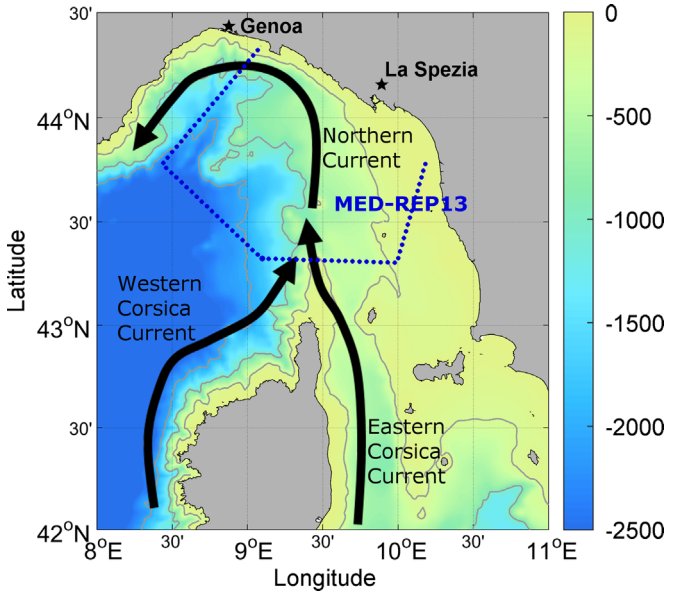

Fig. 1. General circulation in the Ligurian Sea and adjacent waters. The dotted polygon in blue delimits the region investigated during the MED-REP13 field experiment. Thin grey lines denote bathymetry contours for the 200 m, 1000 m and 2000 m depth levels as defined in the GEBCO One Minute Grid dataset (www.gebco.net). Unless stated differently, the same dataset is used in all the following plots. (For interpretation of the references to color in this figure legend, the reader is referred to the web version of this article.)

Lions (Allou et al., 2010; Flexas et al., 2002; Hu et al., 2011; Kersalé et al., 2013; Petrenko, 2003) or along the Catalan shelf (Rubio et al., 2005; Tintoré et al., 1990) through dedicated in-situ and modeling studies.

In the Ligurian Sea the information on eddies is sparse and mostly derives from a variety of modeling studies (Casella et al., 2011; 2014; Echevin et al., 2003; Taillandier et al., 2006) which, in particular, show that eddies may occur throughout most of the Ligurian Sea in association with the NC both along the coast (Casella et al., 2011, 2014) and in the open-sea area of the Gulf of Genoa (Echevin et al., 2003; Taillandier et al., 2006). In particular, in the northeastern sector of the Ligurian Sea investigated here, Casella et al. (2011) tracked, but did not describe in their simulations several anticyclonic eddies associated with the meanders of the NC that did not penetrate below 120 m. Unfortunately, in situ observations of these anticyclonic eddies are limited in number and coverage: Schroeder et al. (2011) indicated the presence of an anticyclonic recirculation in 2008 around 9°E, 44°N, where the NC appeared to bifurcate. The recirculation was described by the trajectories of few trapped surface drifters, therefore there is no information regarding neither the recirculation's vertical structure nor its temporal evolution. In August 2010, an anticyclonic eddy was partially captured around 9°E, 44.1°N by the observations carried out during the Recognized Environmental Picture (REP) 2010 experiment (Alvarez et al., 2013): measurements indicated a low-density core, with a minimum in salinity around 50 m (~37.7) and values still below 38.4 at 160 m, which was the maximum depth of available measurements.

The repeated indication of an anticyclonic eddy in the area offshore La Spezia (Alvarez et al., 2013; Schroeder et al., 2011) invites to hypothesize that this structure may not be a sporadic feature but rather a particular recurrent pattern.

Permanent or recurrent circulation patterns are of wide interest in oceanography. This is because the knowledge of their existence, physical structure and evolution improves the predictability of the local circulation allowing to foresee their impact on biogeochemistry and the local ecosystem (Abella et al., 2008; Casella et al., 2014). Nevertheless to date very little is known about the characteristics of the eddy observed repeatedly in the northeastern Ligurian Sea, as a detailed hydrographic study is not yet available.

Of the dynamical properties that characterize an eddy, vertical velocities are of particular interest, as they have important consequences (in terms of the vertical transport) for the biology and chemistry (Shearman et al., 2000). However, because the order of magnitude of vertical velocities in the ocean is smaller than few mm s^{-1}, they are difficult to quantify from in situ measurements and several methods have been documented in the literature to derive them indirectly from observations. Derivations of vertical velocities based on the Q vector formulation of the omega equation (Shearman et al., 2000) has been used by several authors (i.e., Pascual et al., 2002; Ruiz et al., 2009), although the magnitude of the diagnosed vertical velocities is very sensitive to the resolution of the observations (Buongiorno Nardelli et al., 2012). Other studies made use of numerical models coupled to a low pass digital filter (Shearman et al., 2000; Viúdez et al., 1996) or were configured to assimilate in situ and/or satellite observations (Li et al., 2008; Moore et al., 2009). While data assimilation allows accurate analysis and realistic forecasts, its outcomes vary with changing model configurations (i.e., grid resolution, assimilation techniques, parametrizations, boundary and initial conditions) thus increasing the number of uncertainties in the model's estimates of vertical velocities (Buongiorno Nardelli et al., 2012). Finally, estimates of the three-dimensional circulation patterns, including vertical velocities, have also been obtained through diagnostic runs of ocean models (i.e., Blumberg and Mellor, 1983; Chu et al., 2005; Russo et al., 2009; Zavatarelli, 2002). In this approach, first initial and boundary conditions are reconstructed from the available observations (i.e., through optimal interpolation) and the model is run with fixed temperature and salinity fields. Second, the model is run for a limited number of iterations with fixed boundary conditions derived from the previous stage. In this study, vertical velocities were estimated using a diagnostic setup of ROMS. Clearly, as long as direct observations of the vertical velocities are not possible, the exact level of representativeness of the calculated vertical motions remains unknown (Buongiorno Nardelli et al., 2012; Samuelsen et al., 2012).

This study makes use of a data set collected during the Mediterranean REP 2013 (MED-REP13) field experiment in the northeastern sector of the LPB, to provide a detailed description of the physical and dynamical characteristics of an anticyclonic eddy similar to the ones evidenced in the past by drifters and numerical models. The field experiment aimed at investigating the operational feasibility and the benefits of using an observational network of different platforms to characterize the marine environment. Although the scope of the experiment was different from the objectives of the present study, the campaign allowed the collection of an extensive dataset of temperature, salinity and current measurements in the region offshore La Spezia, illustrating the potential of integrating information from a heterogeneous ocean observing network in observational oceanography.

Results reveal that the anticyclone occupies most of the water column penetrating the thermocline down to at least 300 m. Up to the authors' knowledge, it is the first time that an anticyclonic eddy with these characteristics is observed in the northeastern Ligurian Sea. Exploiting the synergism between our in situ observations and other existing datasets, we hypothesize its formation mechanism, and discuss it frequency of occurrence. The manuscript is organized as follows: the multiple sampling platforms used in this study are described in Section 2, while the main results and their discussion are given in Sections 3 and 4 respectively. Finally, Section 5 summarizes and concludes the work.

2. Data and methods

2.1. In-situ temperature and salinity observations

The MED-REP13 field experiment was conducted with the *NR/V Alliance* of the Center for Maritime Research and Experimentation (CMRE), on 5–20 August 2013 in a marine area offshore La Spezia (Figs. 1 and 2). The sampled region was nearly rectangular with approximately 90 km * 70 km in the along-shore and cross-shore directions, respectively. Oceanographic measurements were collected during the periods of 5–9 August and 16–20 August. Measurement sites are marked in Fig. 2. During 5–9 August (Fig. 2a), 13 Conductivity Temperature Depth (CTD) casts were performed with a SBE911 probe along two parallel tracks spaced about 40 km apart. The two transects were oriented orthogonally to the shelf-break at depths ranging 100–1000 m, along which CTD stations were spaced approximately 10 km from each other. Where possible, CTDs were cast till a maximum depth of 600 m, except for one CTD that was cast till 1000 m depth. The same locations were re-sampled with equivalent criteria during 16–20 August (Fig. 2b).

CTD casts were complemented with temperature and salinity measurements from a towed ScanFish MKII vehicle equipped with a SeaBird 49 CTD, and samples gathered by a fleet of one deep and two shallow Slocum gliders. The ScanFish was towed twice along the periphery of the surveyed domain (Fig. 2a), between 5 Aug 17:43 – 6 Aug 14:28 and between 07 Aug 18:22 – 08 Aug 14:28 (all times are in UTC). The instrument followed a vertical sawtooth trajectory between 5 m and 240 m depth, with horizontal and vertical speeds of 3 and 1 m s^{-1} respectively, allowing a sampling horizontal resolution better than 3 km. The deep glider was programmed to dive between 15 m and approximately 500 m, while the shallow gliders sampled the water column between 15 m and approximately 170 m depth. The glider CTD data were collected with a sampling rate of 1 Hz or 0.5 Hz (un-pumped or pumped CTD, respectively). The trajectories followed by the three gliders during the two periods of observations (i.e., 5–9 August and 16–20 August) are marked in Fig. 2a and b.

Additionally, historical temperature and salinity profiles were retrieved over the eddy area from the World Ocean Database 2013 (WOD13, Boyer et al., 2013). WOD13 is hosted at the *NOAA* National Oceanographic Data Center (https://www.nodc.noaa.gov/OC5/WOD13/), and contains a collection of temperature and salinity measurements recorded in the World's oceans from different platforms (i.e., CTD, XBT, CTD float profilers, gliders) for the years 1973–2013 (MED-REP13 data are not included). To evaluate the climatological water properties in the eddy region, temperature and salinity profiles were extracted for August, but also July and September in order to increase the number of measurements available in the area, and thus the representativeness of the mean field.

2.2. Ocean current measurements from the vessel mounted Acoustic Doppler Current Profile and drifters

Along-ship-track ocean current measurements were acquired during the whole campaign with a vessel mounted 75 kHz Ocean Surveyor Acoustic Doppler Current Profiler (ADCP). The ADCP was configured to measure currents at 40 depths ranging between 30 m and 650 m. Depth layers were equally spaced every 16 m. ADCP data acquired between 5 and 9 August 2013 were processed and averaged to obtain one measurement every two minutes. ADCP measurements acquired on 7 August, when the ship transited close to the center of the anticyclonic eddy, are used to describe the horizontal velocities within the eddy (see Figs. 12 and 13), to locate the position of its center and to measure the eddy's horizontal extent. Using the methodology described by Garau et al. (2006), the eddy center was identified as the point where the number of intersections of the radial directions between pairs of ADCP velocity vectors was highest. The eddy's radius, instead, was identified as the distance from the eddy center where surface (i.e., 30 m) horizontal velocities reached their maxima.

Additionally, ADCP measurements for each depth layer were used to calculate the stream function by using a Bayes least square estimate resulting from:

$$\hat{\psi}\left(\vec{x}\right) = \arg\min_{\psi}\left\{\sum_{i=1}^{N}\frac{\left(\frac{\partial}{\partial y}\psi\left(\vec{x}_i\right)-u_i\right)^2}{2\sigma^2}+\frac{\left(\frac{\partial}{\partial x}\psi\left(\vec{x}_i\right)+v_i\right)^2}{2\sigma^2} + \iint\psi\left(\vec{y}\right)C^{-1}\left(\|\vec{y}-\vec{x}\|\right)\psi\left(\vec{x}'\right)dxdy\right\} \quad (1)$$

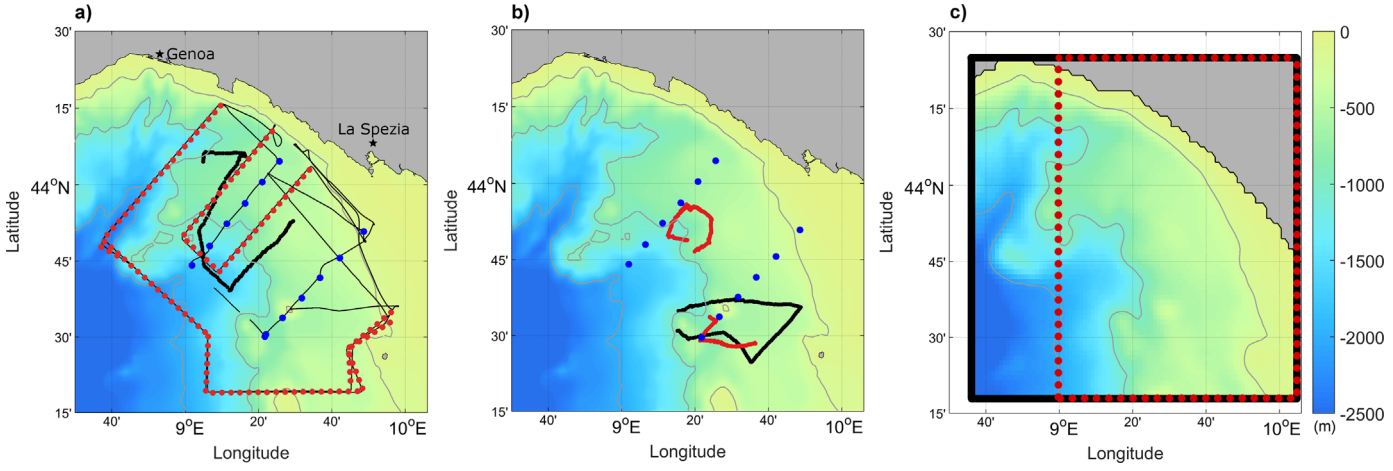

Fig. 2. Locations of the in situ measurements during MED-REP13 for the two periods 5–9 August 2013 in (a) and 16–20 August 2013 in (b). Background color denotes bottom topography. Sampling platforms are coded as follows: blue dots denote shipborne CTD stations; the red-dotted line denotes the track of the towed ScanFish MKII vehicle; thick black lines denote the trajectories of the deep glider, while thick red lines denote the trajectories of the shallow gliders; thin black lines in panel (a) delineate the trajectory of the ship for which ADCP current measurements are available. Panel (c) shows the ROMS bottom topography (Smith and Sandwell, 1997) as well as the extensions of the domains utilized in the model setup. The black polygon denotes the domain size in the first stage of the model setup, the dotted red polygon denotes the domain size adopted in the second stage of the model setup. In all panels, bathymetry contours for the 200 m, 1000 m and 2000 m depth levels are marked with thin grey lines. (For interpretation of the references to color in this figure legend, the reader is referred to the web version of this article.).

Table 1
Times (UTC) and coordinates (Longitude and Latitude) of drifter deployments and last available positions.

Drifter ID number	Deployment		Last position	
	Date & time	Coordinates	Date & time	Coordinates
300234060607060	14 Aug 2013 02:48:43	9.42°E, 43.55°N	24 Aug 2013 08:58:33	9.13°E, 43.99°N
300234060506980	14 Aug 2013 03:05:13	9.47°E, 43.59°N	18 Aug 2013 07:51:38	9.18°E, 44.28°N
300234060601040	14 Aug 2013 03:43:45	9.56°E, 43.66°N	03 Sep 2013 23:06:14	8.64°E, 44.34°N
300234060502970	14 Aug 2013 03:55:22	9.49°E, 43.62°N	17 Aug 2013 11:18:14	8.95°E, 44.25°N

where $\{u_i, v_i\}_{i=1}^{N}$ are the observed horizontal components of the velocity at position $\vec{x}_i$, σ is an observational error associated to the observations and $C(\,.\,)$ is a Gaussian covariance matrix with a decorrelation scale of 37 km. The decorrelation scale was calculated from the horizontal covariogram of the observations, which relates, for a stationary stochastic process, the covariance between the locations of two measurements with their relative horizontal distance. The numerical procedure employed to solve the minimization problem Eq. (1) is described in Alvarez and Mourre (2012). Velocity fields from the stream function are used for a synoptic and highly resolved three-dimensional characterization of circulation in the study area, but also for a comparison of outputs from the Regional Ocean Modeling System (ROMS).

Information on surface circulation was also obtained from Lagrangian measurements. On 14 August, between 2:48 AM and 3:55 AM (UTC), four surface drifters (model MD03i) drogued at 1 m depth were deployed in the study area. The dates and coordinates of their deployment and last available positions are summarized in Table 1. Their daily positions (Fig. 3) were retrieved via the Iridium Satellite communication network. All surface drifters were operative at least till 17 August. Poulain et al. (2009) indicated that the drifting velocities of 1-m-drogued drifters are affected by the wind speed by only 1% of its magnitude.

2.3. Sea surface chlorophyll concentration, satellite altimetry and surface winds

Standard-mapped images, level-3 three-day composites of Aqua-MODIS Chlorophyll *a* (Chl *a*) concentrations, were retrieved from the Distributed Active Archive Center (http://oceancolor.gsfc.nasa.gov) for 7–9 August. Satellite products are processed by the Goddard Space Flight Center and projected on a regular spatial grid of 4 km. The specific three-day composite image was chosen because it allowed the maximum coverage of the eddy area, yet remaining close enough in time to the timing of in-situ measurements acquired during 5–9 August. Limitations in satellite data coverage (partly due to cloud cover during the field experiment and partly due to the low quality of the satellite imagery) as well as the poor surface thermal signature of the anticyclonic eddy of interest prevented a fruitful exploitation of sea surface temperature (SST) imagery.

Daily delayed-time values for the zonal and meridional components of absolute geostrophic velocities, computed from absolute topography, and re-sampled on a regular grid, were extracted for the time period between January 1993 and December 2013 from the Aviso satellite altimetry webpage (http://www.aviso.oceanobs.com/duacs/). Altimetry gridded maps derive from the merging of data over several altimeter missions providing a consistent and homogeneous data set for the Mediterranean Sea at a resolution of 1/8°. Therefore, they are too smooth to resolve the small (order of 10–100 km) and coastal features (Amores et al., 2013; Birol et al., 2010; Escudier et al., 2013) evidenced in the in situ ADCP data. Nevertheless they can provide useful information about the larger scale patterns and their dynamical evolution.

Hourly measurements of winds at 10 m above the sea level, at a

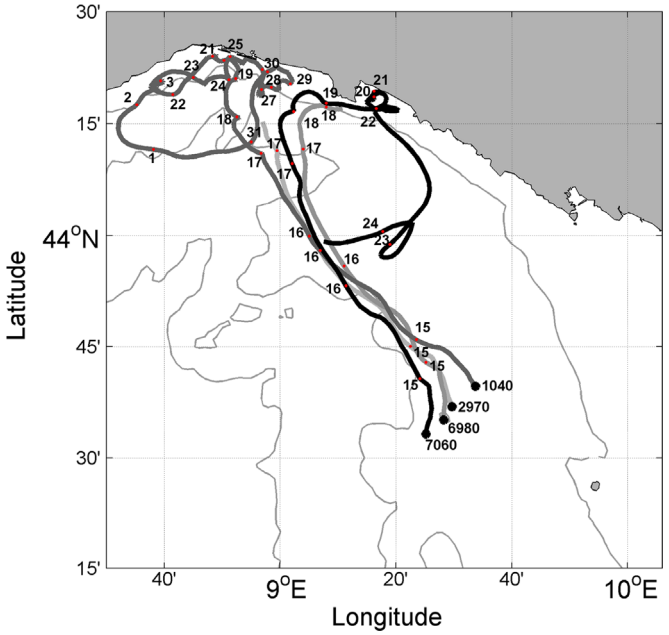

Fig. 3. Trajectories followed by four surface drifters deployed on 14 August 2013 between 2:48 AM and 3:55 AM (UTC). Each deployment location is shown with bold black dots together with the last four digits of each drifter ID number (Table 1). Each start of a new day between 15 August and 3 September are also denoted along the trajectories. Thin grey lines denote bathymetry contours for the 200 m, 1000 m and 2000 m depth.

horizontal resolution of 6.5 km were obtained from the Consortium for Small Scale Modeling (COSMO, Baldauf et al., 2011) for 1 July-21 August 2013. The COSMO-Model is a non-hydrostatic limited-area atmospheric prediction model. It has been designed for both operational numerical weather prediction and various scientific applications. A thorough description of the model system is also given in the documentation available at the COSMO website (www.cosmo-model.org).

2.4. Configuration and setup of ROMS diagnostic simulations

ROMS is a three-dimensional, free-surface split-explicit primitive equation model. Vertical and horizontal coordinates are discretized in terrain-following curvilinear coordinates (i.e., sigma-layers) using high-order finite differences. ROMS characteristics and time stepping algorithm are described in detail by Shchepetkin and McWilliams (2005). The Generic Length Scale (GLS) vertical mixing parameterisation (Umlauf and Burchard, 2003) is activated using the Kantha and Clayson stability function. To test the effects of different mixing parameterisations on the prediction of vertical velocities, sensitivity simulations were performed using the Large-McWilliams-Doney (LMD) vertical mixing scheme (Large and Gent, 1999), but results were comparable in all cases.

Similarly to the approaches of Blumberg and Mellor (1983), Chu

et al. (2005) and Russo et al. (2009), results presented and discussed below are derived from a two-stage model setup. In the first stage the model domain included the Ligurian Sea from 43.3°N to 44.4°N and from 8.6°E to 10.1°E at 1.8 km resolution (Fig. 2c), and 32 sigma-coordinate vertical layers stretched to increase resolution close to the surface. In this model configuration there were three open lateral boundaries located on the western, eastern and southern sides of the domain. Radiation boundary conditions were implemented for the barotropic and baroclinic velocity components in order to radiate instabilities out of the domain. Moreover, volume conservation was enforced and gradient boundary conditions were adopted for the free surface. Bottom topography was based on the global topography dataset at 2' resolution (Smith and Sandwell, 1997). On the eastern boundary the bathymetry has been clipped to 50 m in order to prevent spurious numerical instabilities generated by the very shallow shelf (less than 100 m) which characterizes this portion of the domain. Changes in topography due to the clipping to 50 m are limited to the small and shallow area in the southeastern sector of the coast which is far from the main dynamical setting of the eddy.

The model was run in a diagnostic configuration using temperature and salinity observations from the period 5–9 August. According to the study of Alvarez and Mourre (2012) in the Ligurian Sea, in this 4-day time period in situ observations were assumed synoptic, in the sense that the temporal variability of water properties in the 4-day interval can be considered much smaller that the variations related to the large scale structures. In situ temperature and salinity measurements were objectively analyzed and interpolated onto a regular 3D grid. The interpolation grid was characterized by a horizontal resolution of about 7 km, while along the vertical dimension 63 levels were defined from the surface to the bottom with decreasing resolution. In the first 300 m, the average vertical resolution was approximately 10 m. Based on the horizontal covariogram the correlation length used in the interpolation was estimated to be 37 km.

The model was initialized with zero free surface and zero momentum and configured for a diagnostic simulation where temperature and salinity measurements from the 3D-grid constructed as described above, were kept fixed in time. With this configuration the model was thus used to compute the free-surface and momentum that balances the frozen density state derived from in situ data (see also Blumberg and Mellor, 1983; Chu et al., 2005). After a short run of 20 modeling days the model reached and maintained quasi equilibrium and its outputs of temperature, meridional and zonal components of velocity as well as sea surface height were used to set the boundaries and initial conditions of the second stage of the model setup. The chosen 20-day spin up time is in agreement with the earlier studies of Blumberg and Mellor (1983).

In the second stage of the simulations, the model's horizontal resolution was kept to 1.8 km while the model's western boundary was shifted eastwards to 9°E (see Fig. 2c), so that the main flow driven by the NC (see Section 3.2) entered and exited the model domain perpendicularly to the western boundary. This configuration avoided spurious recirculation cells generated in the western portion of the study area, where the main oceanographic structures were not sampled adequately by the available in situ observations. The algorithm proposed by Marchesiello et al. (2001) combining radiation and nudging (with a time scale of one day) is implemented to calculate the baroclinic flows through the lateral open boundaries, using external values from the restart file of the first model setup. Chapman boundary condition was adopted for the free surface together with a strong (i.e., one day) interior grid nudging for temperature and salinity. Sensitivity tests show that with larger nudging temporal scales differences between observations and simulation outcomes increase. The model was initialized with the fields obtained from the first stage of the model configuration and run for two months, until the dynamic equilibrium, evaluated in terms of kinetic energy of the system, was reached. In the following, results from the 60th model day are presented. Due to the application of a strong interior grid nudging (i.e., one day), the velocity fields simulated by ROMS are dynamically consistent with temperature and salinity, but not in full geostrophic balance because the model's momentum advection and diffusion terms are not null.

Diagnostic simulations with the ROMS model were primarily used to estimate vertical velocities developing within the eddy. However, they also provide the means to obtain, from the non-uniform distribution of available observations, a three-dimensional and dynamically consistent characterization of the physical and dynamical oceanographic conditions in the interior of the domain with a relatively simple technical set up and reasonable computational cost.

3. Results

3.1. Description of water masses

Temperature and salinity measurements collected in the MED-REP13 study area by all sampling platforms (i.e., gliders, ScanFish and CTD casts) during both periods of oceanographic observations (5–9 August 2013 and 16–20 August 2013, Fig. 2) allow for the identification of the main water masses that characterize the LPB basin, in agreement with the general hydrographic conditions described in the literature. Temperature-salinity diagrams (Fig. 4) are used to represent water properties observed during the two sampling periods. Moreover, given the particularly dense distribution of the data collected during the first sampling period, temperature and salinity properties for 5–9 August 2013 are also displayed in Fig. 5 for a three dimensional overview of the sampling area.

The densest (greater than 29, Fig. 4) waters are at depths greater than around 300 m and exhibit the main characteristics of the Levantine Intermediate Water (LIW) clearly identified by a temperature maximum (i.e., values of 13.2–13.8 °C) and salinities greater than 38.6. Measurements shallower than the LIW indicate two distinct types of water. The first water type occupies the left half of the TS diagram (Fig. 4), and can be identified with the Modified Atlantic Water (MAW), here characterized by very low salinity (37.7–38.0 PSU) and warm temperatures (13.5–26 °C) between the thermocline and ~300 m. As the MAW is advected in the LPB with the WCC and then the NC, its characteristic temperature and low salinity values are observed in all measurements taken along and to the east of the main NC path (Fig. 5). The second type of waters has temperature ranges similar to those described above, but higher salinities ranging 38.1–38.3. These more saline waters occupy the right half of the TS-diagram (Fig. 4) and reflect the MAW found closer to the center of the LPB cyclonic gyre (Fig. 5). Interestingly, during the first sampling period (5–9 August 2013) the presence of these saltier MAW is detected by the northernmost CTD casts only (red dots in Fig. 4a), but by both CTD transects during the second observational period (16–20 August 2013 in Fig. 4b) reflecting the change of water properties linked to the presence and then northwards movement of the anticyclonic eddy (see Discussion section below).

3.2. Large scale circulation patterns

The velocity field derived from ADCP measurements from 5 to 9 August provides a rather detailed description of the circulation in the area. Results at 30 m, i.e., the first depth layer sampled by

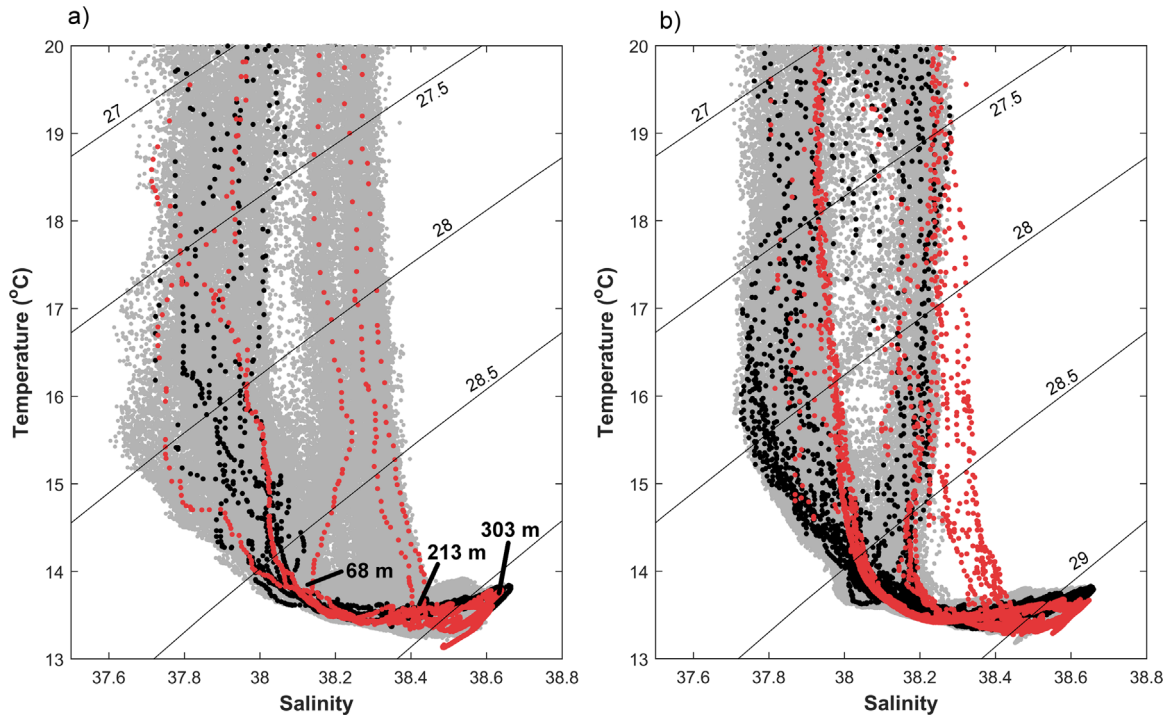

Fig. 4. TS diagrams based on the measurements collected during the two periods 5–9 August 2013 in (a) and 16–20 August 2013 in (b) by gliders and/or ScanFish depending on the period of observations (grey dots) and those obtained from CTD casts in the northernmost (red dots) and southernmost (black dots) transects shown in Fig. 2. In (a) the approximate depths of the most significant features of the diagram are also given. Oblique lines denote isopycnals. (For interpretation of the references to color in this figure legend, the reader is referred to the web version of this article.).

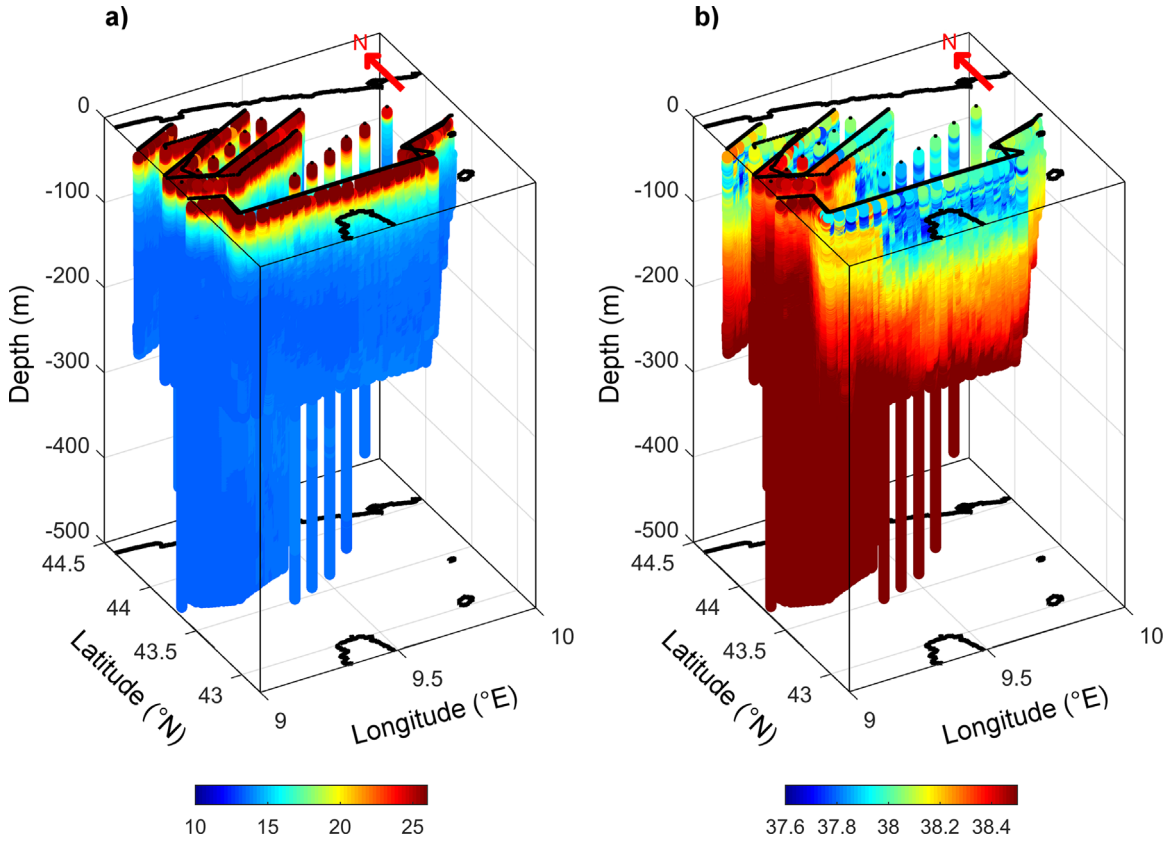

Fig. 5. Three-dimensional view of temperature (a) and salinity (b) values observed during the first period of the sea trial (5–9 August 2013). Black dots at the surface mark the sampling locations as coded in Fig. 2a. An animated three-dimensional view of the same dataset is available in the Supplementary material.

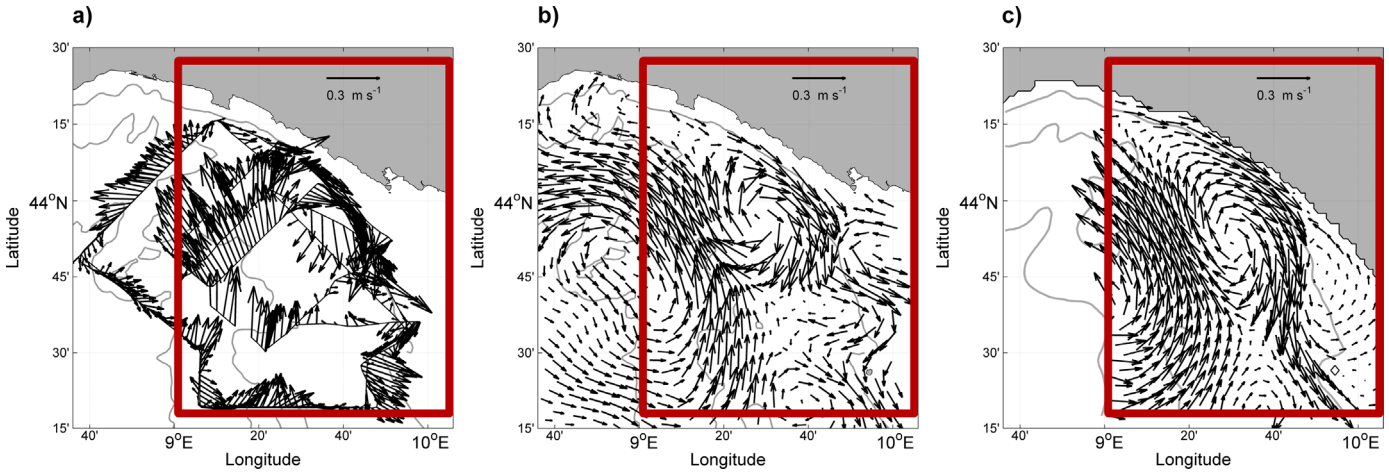

Fig. 6. a) Horizontal velocity field as obtained from ADCP current measurements at 30 m between 5 and 9 August 2013. b) Horizontal velocity field derived from the stream function calculated using the ADCP measurements shown in panel a. c) Currents simulated by ROMS at 30 m. Note that the coastline in the model is the result of the topographic clipping to 50 m (see Section 2.4). In all panels the red rectangle marks the ROMS model domain and thin grey lines denote bathymetry contours for the 200 m, 1000 m and 2000 m depth levels. Note that in c) grey lines denote the same contours but for the model's bottom topography. (For interpretation of the references to color in this figure legend, the reader is referred to the web version of this article.).

the ADCP, are shown in Fig. 6a. The most evident circulation feature is the NC, shown as an intense ($\sim$0.4 m s^{-1}) northwestwards current that flows across most of the study area following the 1000 m bathymetry contour around the shelf-break, and that exits the domain to the northwest. The width of the NC is estimated to be around 36 km. Moreover, ADCP measurements and the derived stream function (Fig. 6b) clearly indicate the cyclonic (i.e., counterclockwise) circulation that characterizes the southwestern sector of the Ligurian Sea (Millot, 1999). Between the northeastern edge of the NC and the coast, around 9.5°E, 43.9°N at water depths of $\sim$500 m, there is a clear indication of an anticyclonic (i.e., clockwise) eddy centered at about 21 km from the coast, with a radius of 16 km and a slightly elongated shape in the north-south direction. Maximum velocities are observed in the eastern and western side of the eddy ($\sim$0.4 m s^{-1}), which appears to be integrated into the eastern edge of the NC flow. Conversely, in the northern and southern sectors of the eddy the flow is weaker, ranging 0.1–0.2 m s^{-1}. Based on ADCP observations and water properties within the eddy (described below), this circulation structure extends vertically up to approximately 350 m below the surface.

Qualitative comparison between the circulation patterns described above (Fig. 6a and b) and the results from ROMS simulations (Fig. 6c), shows that the model analysis nicely agrees with the circulation features derived from ADCP data. It is important to note that the two circulation datasets used in the comparison are independent, as ADCP observations were not used in the numerical procedure. The simulated current field reproduces an intense ($\sim$0.4 m s^{-1}) northwestwards current that compares very well, in terms of location, direction, width and intensity with the main characteristics of the NC described above. Particularly relevant to the objectives of this study is the ability of the model to simulate the anticyclonic eddy evidenced in the in situ observations.

The position of the eddy center in the modeled surface current and its radius are calculated as for observations. The model reproduces an eddy that is slightly more elongated in the northwest-southeast direction than in the observations with its center around 9.5°E, 43.87°N (Fig. 6c) and an average radius of 18 km. Small discrepancies between the observed and modeled eddy are likely due to the simplified model's representation of bathymetry but also due to the fact that ADCP current measurements used to calculate the stream function provide a better temporal and spatial coverage of the region of interest than the in-situ temperature and salinity measurements used to initialize and force the model (the spatial coverage of the two datasets are shown in Fig. 2). Differences in the location and size of the observed and modeled eddy do not influence the conclusions of this study.

A quantitative assessment of the performance of ROMS to diagnose the dynamics in the eddy is provided by measuring the similarity between all the in-situ ADCP current measurements available along the ship track between 5 and 9 August 2013 contained within the boundaries of the model's domain (Fig. 6a) and model results interpolated onto the locations of the in situ ADCP measurements. This similarity assessment is done using Taylor diagrams (Taylor, 2001) which represent the statistical relationship between the two fields. Model results that agree well with observations will have similar standard deviation, relatively high correlation and small Root Mean Square Deviation (RMSD) values between model outputs and observations. In the calculations, the zonal and meridional components of observed and simulated current velocities are from depths equal and shallower than 110 m, because for depths greater than 110 m, comparison with observations indicates that the model's RMSD becomes larger than the velocity magnitudes measured by the ADCP.

Simulated zonal velocities (U_roms in Fig. 7a) have a RMSD of 0.07 m s^{-1} and are positively correlated to observations (correlation coefficient is 0.57). The standard deviations of the two datasets are also comparable in magnitude (0.08 m s^{-1} and 0.07 m s^{-1} for U_obs and U_roms, respectively). Regarding the model's estimate of the meridional velocities (V_roms in Fig. 7b) the correlation coefficient is higher than in the previous comparison (i.e., 0.75), with a RMSD value of $\sim$0.08 m s^{-1}. The calculated standard deviations in the observed and modeled fields (V_obs and V_roms, respectively) are 0.12 m s^{-1} and 0.11 m s^{-1}. Considering the limitations involved in the dataset comparisons (i.e., the different temporal and spatial resolution of the data, or the effect of a slightly displaced eddy in the two datasets), results represented on the Taylor diagram confirm quantitatively the good agreement between observed and modeled circulation shown in Fig. 6.

Model results allow a uniform three-dimensional coverage of the whole area, and thus the calculation of volume transports across the main circulation pathways of the region but also across the eddy. Transport was calculated along the transects shown in Fig. 8 and over the depth range 30–300 m, allowing for a comparison with estimates obtained from the stream function (values between parenthesis in Fig. 8). An uncertainty of $+/-0.02$ Sv for

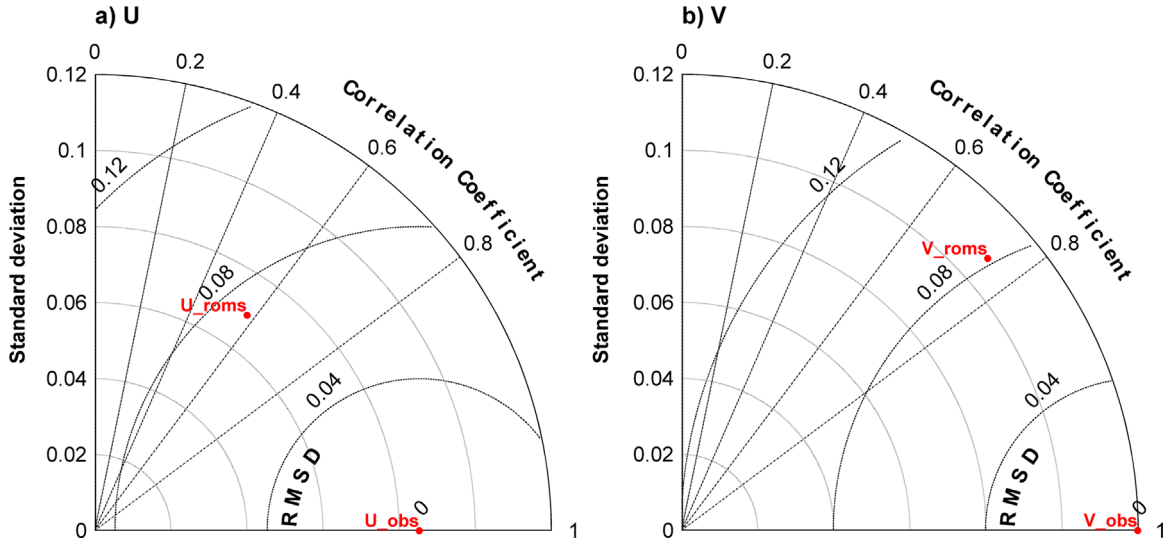

Fig. 7. Taylor diagram for the a) zonal (i.e., east-west) and b) meridional (north-south) components of velocity, calculated from modeled (U_roms and V_roms) and observed (U_obs and V_obs) values. In a) correlations are calculated with respect to U_obs, which explains why U_obs is placed on the axis of correlation = 1. The same principle explains the position of V_obs in panel b). Calculations are based on current velocities till the 110 m depth layer.

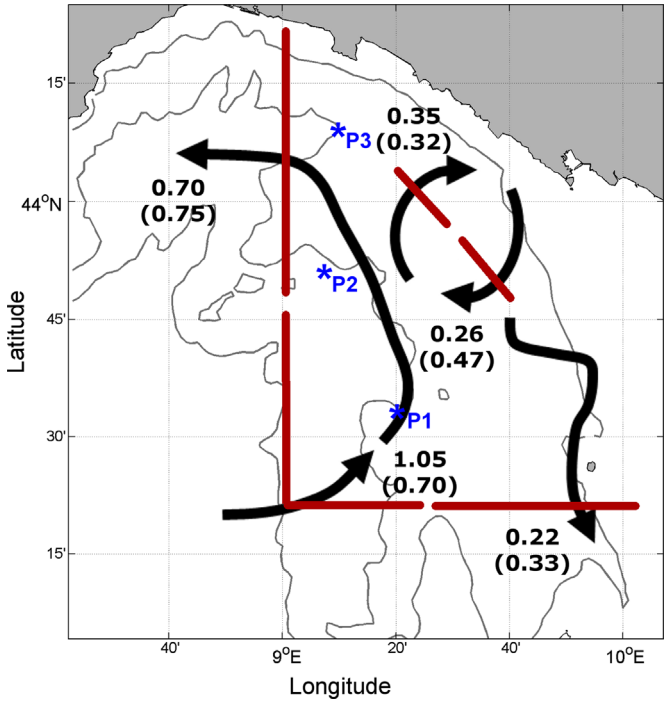

Fig. 8. Circulation schematics and mass transport across the study area as from ROMS model outputs and from the calculated stream function (values in parentheses). Values are calculated over the 30–300 m depth layer, and across each section marked in red. All transport values are reported in Sv ($1\ Sv = 10^{-6}\ m^3\ s^{-1}$). The error in the model's transport estimates is equal to ± 0.02 Sv. Thin grey lines denote contours for the 200 m, 1000 m and 2000 m depth levels. Blue stars denote the locations of the three reference profiles (P1, P2, P3) used for Fig. 10. (For interpretation of the references to color in this figure legend, the reader is referred to the web version of this article.).

the transport estimates has been obtained by computing the RMSD of the model velocities at the ADCP observation locations. Overall, there is one main region of inflow located in the southwest corner of the domain, where the southern branch of the NC entering the study area and the northwards flowing WCC lead to a total surface transport of 1.05 Sv. Estimates from the stream function result in a transport value (0.70 Sv) lower than the model estimates (1.05 SV) due to the overestimation by the model of the horizontal currents below 100 m. On the other hand, there are two main regions of outflow: the first is located to the southeast where the model reproduces a coastal current flowing southwards with an estimated transport of 0.22 Sv; the second region of outflow is located to the northwest of the domain, and is associated with the NC. Here the current exits the study area due west with a transport of 0.70 Sv. The same calculations were repeated to estimate the transport within the eddy area, which on average accounted for 0.30 Sv. Estimates from the stream function indicate a mean transport (0.39 Sv) higher than the model, as the latter underestimates the intensity of horizontal velocities in the shallower layers of the eddy, especially in the southern section. Along the Italian and French coast, the NC has been reported to have a maximum flux of 1.5–2 Sv down to 700 dbar (Albérola et al., 1995; Conan and Millot, 1995; Sammari et al., 1995; Schroeder et al., 2008). Therefore, for the purpose of an additional validation of the model estimates, we calculated the 0–700 m transport across the section cutting through the northern portion of the NC and found a value of 1.31 Sv, which is comparable with the transport estimates provided by previous studies.

3.3. *The anticyclonic eddy*

To characterize the main salinity and temperature characteristics outside and within the eddy area, we use model outputs which, due to the chosen diagnostic configuration, reflect observations and allow a uniform three-dimensional coverage of the area. Modeled values were extracted along the zonal section crossing the eddy center at 43.87°N (Fig. 9). Moreover, profiles of modeled temperature, salinity and the corresponding density at the eddy center (9.5°E, 43.87°N) and for three locations outside the eddy area (used as reference in the comparison) are shown in Fig. 10.

The most evident signature of the anticyclonic eddy is the deepening of the isotherm and isohaline surfaces (Fig. 9a and b), which reach their maximum depths around 9.5°E. To the east and west of 9.5°E, isolines are tilted and rise to the surface, so that the horizontal extent of the area influenced by the eddy is maximum close to the surface decreasing with depth.

The temperature section (Fig. 9a) and vertical profiles (Fig. 10a) show that the eddy signature is limited to depths shallower than about 100 m where temperatures range between 14 °C and 24.7 °C

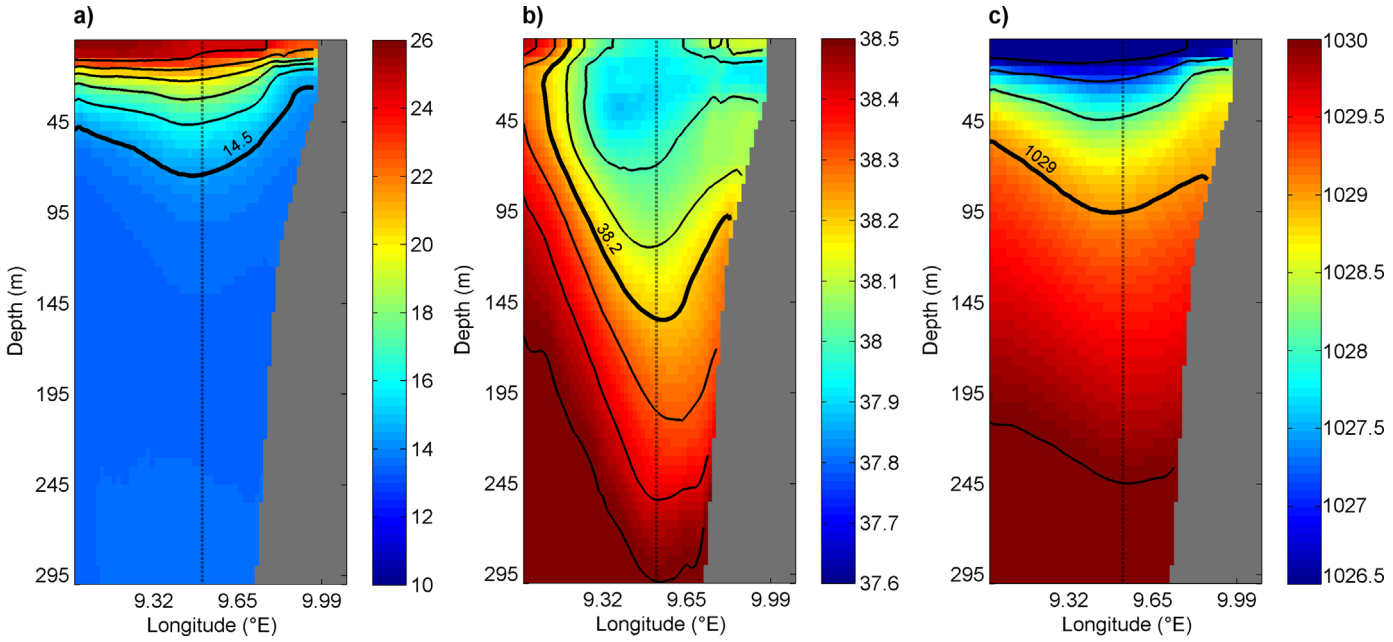

Fig. 9. Modeled temperature (a) salinity (b) and density (c) sections along latitude 43.87°N which crosses the eddy center estimated in the ROMS results. For reference, in panel (a) isotherms between 14.5 °C and 19.5 °C are marked every 1 °C interval. The 14.5 °C isotherm mentioned in the text is marked with a bold line. In panel (b) isohalines between 37.8 and 38.8 are marked every 0.2; the 38.2 isohaline mentioned in the text is marked with a bold line. In (c) contours denote the 1 density interval. As reference, the thin dashed vertical line marks the center of the eddy, at 9.5°N. Areas shaded in grey mark the sea floor.

close to the surface. Between 10 m and 70 m the temperature gradient is maximum, as temperatures decrease at a rate of approximately 0.16 °C m^{-1}. Considering the 14.5 °C isotherm (marked in Fig. 9a), the difference between its depth at the center and its depth at the western edge of the eddy is of approximately 25 m. Below 100 m temperatures remain rather constant and close to 13.5 °C, which is the typical temperature of the MAW at this depth (Albérola and Millot, 2003). Conversely, the salinity section (Fig. 9b) and vertical profiles (Fig. 10b) indicate that the core of the eddy can be traced down to approximately 350 m, occupying most of the 500 m deep water column. Below this depth, in fact, the salinity profile at the center of the eddy (Fig. 10b) tends to approach the salinity profile for the regions outside the eddy. In particular, profiles in Fig. 10b show that the low salinities found within the eddy are similar to those present in points P1 and P3 (marked in Fig. 8), indicate that Salinity is minimum (i.e., 37.9) in the first 40 m, and increases progressively with an average rate of 0.002 m^{-1} till 250 m, below which salinity reaches 38.55 and remains close to the region's background values. Considering the 38.2 isohaline (marked in bold in Fig. 9b), the difference between its depth at the center and at the western edge of the eddy is of approximately 125 m. Temperature and salinity fields within the eddy, clearly reflect the water properties of the MAW transported by the NC (Fig. 5). Comparison between the sections and profiles of temperature, salinity and density shown above clearly indicates that for such eddy, temperature fields can only provide a limited view of its structure, as the eddy signature can be traced at depths that are much greater than 100 m if the salinity field is considered instead. This is confirmed by the density fields resulting from the temperature and salinity properties described above (Figs. 9c and 10c).

As salinity best highlights water property differences between the eddy and the surrounding waters along the whole water column, comparison between the salinity field from the two periods of observations 5–9 August and 16–20 August (see Fig. 2 for measurement locations) can be used to describe the evolution of the eddy during the time of the trial. For such purpose, model results cannot be used because in the chosen diagnostic configuration the ocean state is not allowed to evolve in time. Salinity fields obtained at 150 m (i.e., the mid-depth of the eddy) after interpolation onto a regular 3D-grid as described in Section 2.4 are shown in Fig. 11 for both periods of observations.

At 150 m, the low salinity area (~38.2) associated with the eddy during 5-9 August (Fig. 11a) is centered around 9.5°E, 43.97°N. Salinity values within the eddy clearly reflect the elongated shape observed in the circulation patterns. Moreover, one can also observe that further south salinity values are in the range of values measured within the eddy suggesting that the eddy may have originated from the south. At the same depth, but 11 days later (16–20 August, in Fig. 11b) a similar low salinity area (~38.2 PSU) is located more to the north, around (9.32°E, 44.08°N) hence indicating that during the time of the cruise the eddy was not stationary but had shifted approximately 29 km northwestwards maintaining a rather constant distance from the coast, with an average drift velocity of 0.03 m s^{-1} (i.e., 2.6 km day^{-1}). The latter position is confirmed by the trajectory of the surface drifter deployed during the cruise. The drifter, which initially followed a northwestern trajectory along the main path of the NC, on 17 August steered eastwards and completed an anticyclonic loop very close to the periphery of the eddy. The center of the drifter loop is around (9.20°E, 44.15°N) hence suggesting that after 20 August, the eddy may have translated further northwest. Comparison between the salinity obtained around the center of the eddy during the two sampling periods suggests that values were lower during 16–20 August (Fig. 11b). The salinity difference most likely derives from the spatial interpolation of a different number and distribution of observations in the area during the two sampling intervals.

A detailed 3-dimensional characterization of the velocity field within the eddy is possible by means of the shipborne ADCP in situ data collected on 7 August, when the ship navigated across the area influenced by the eddy. From SW to NE, following the direction of the ship transect, the velocity vectors at ~30 m (Fig. 12a) indicate a northwards flow of ~0.35 m s^{-1} which decreased gradually to values very close to 0 m s^{-1} around 9.47°E. Continuing NE, the vectors turned southeast, and the intensity gradually increased to ~0.53 m s^{-1}. At the surface the center of

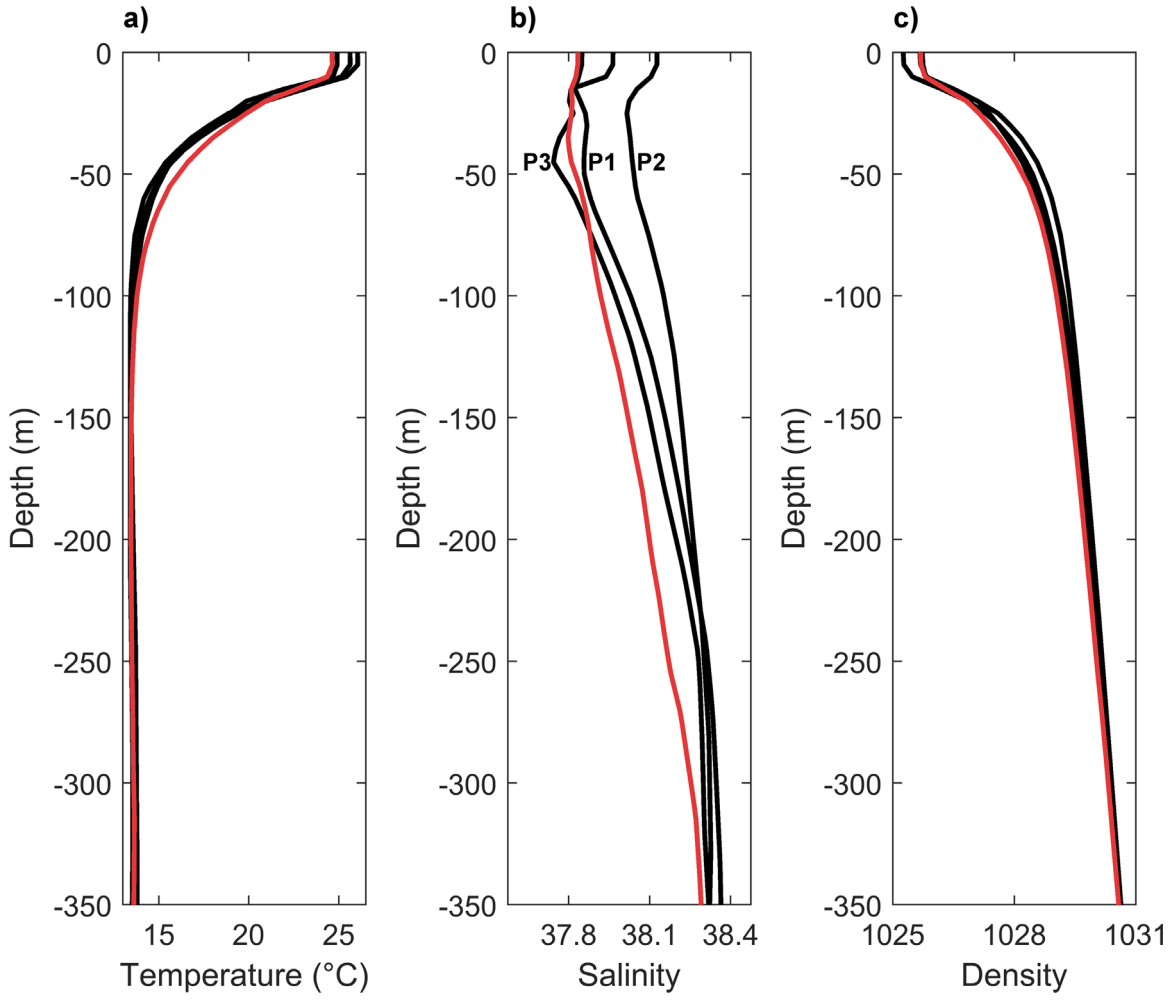

Fig. 10. Vertical profiles of temperature (a), salinity (b) and density (c) at the center of the modeled eddy (9.5°E, 43.87°N, red curves) and outside the eddy (black curves) in three locations outside the eddy, i.e., at point P1: (9.37°E, 43.49°N), point P2: (9.14°E, 43.83°N) and point P3 (9.18°E, 44.17°N), as shown in Fig. 8. (For interpretation of the references to color in this figure legend, the reader is referred to the web version of this article.).

the eddy was located around (9.47°E, 43.95°N), as denoted by the black dot in Fig. 12a. Below the surface, at 150 m depth (Fig. 12b), the velocity vectors indicated weaker velocities, and a similar but more gradual variation in the direction of the flow indicating that at greater depths, the eddy center was further south than at the surface (black dot in Fig. 12a).

The current component normal to the ship's transect, shown in Fig. 13, allows an estimate of the eddy's vertical extension, as well as a description of its subsurface characteristics. Along the transect, the eddy can be identified by the presence of a quasi-vertical axis of symmetry along which horizontal velocities are very close to zero and across which the current component normal to the transect changes sign. Such vertical line can thus be associated with the axis of rotation of the eddy. West of the eddy's axis of rotation velocities are positive (northwestwards) while in the east current velocities are negative (southeastwards). The horizontal extent of the area influenced by the eddy is estimated measuring the distance between the center of the eddy and the point where surface velocities reach their maximum values (i.e., 0.2 m s^{-1}). Using current measurements acquired along the chosen transect, the eddy radius is approximately 16 km in the near-surface, decreasing with depth. Horizontal velocities measured within the eddy decrease with depth, and reach their minimum values around 300–350 m. Below this depth, which can be considered representative of the eddy's maximum vertical extent, measured current velocities are close to the surrounding background values. Above this depth, instead, horizontal velocities increase progressively reaching 0.15 m s^{-1} at 150 m, and reach their maximal velocities in the first 60 m ($\sim 0.23 - 0.30$ m s^{-1}). In agreement with the eddy-structure described previously in modeled temperature and salinity fields (Fig. 9), in situ ADCP measurements clearly evidence that the eddy is characterized by a typical bowl-shape (Dong et al., 2012).

The order of magnitude of vertical velocities in the ocean is smaller than few mm s^{-1}, and is thus difficult to quantify from in situ measurements. Given the large number of uncertainties linked to their calculations (see Introduction) we estimated patterns and magnitudes in vertical velocities from ROMS modeling results, which intrinsically takes into account the full physics of the system but also the particular configuration of bathymetry (i.e., the proximity to the continental slope). Additionally, for a comparison of results, the uniformly spaced temperature and salinity field obtained from the model are used to estimate vertical velocities from the Q vector formulation of the omega equation (Shearman et al., 2000). Vertical velocities obtained from the two methodologies along the zonal section defined along 43.87°N, which intersects the center of the modeled eddy (Fig. 6c), are shown in Fig. 14.

Overall, comparison between the two vertical velocity fields shows a rather good agreement, both in terms of the spatial patterns and magnitudes. Within the core of the eddy (9.25°E – 9.8°E) and at depths shallower than 150 m, absolute vertical velocities

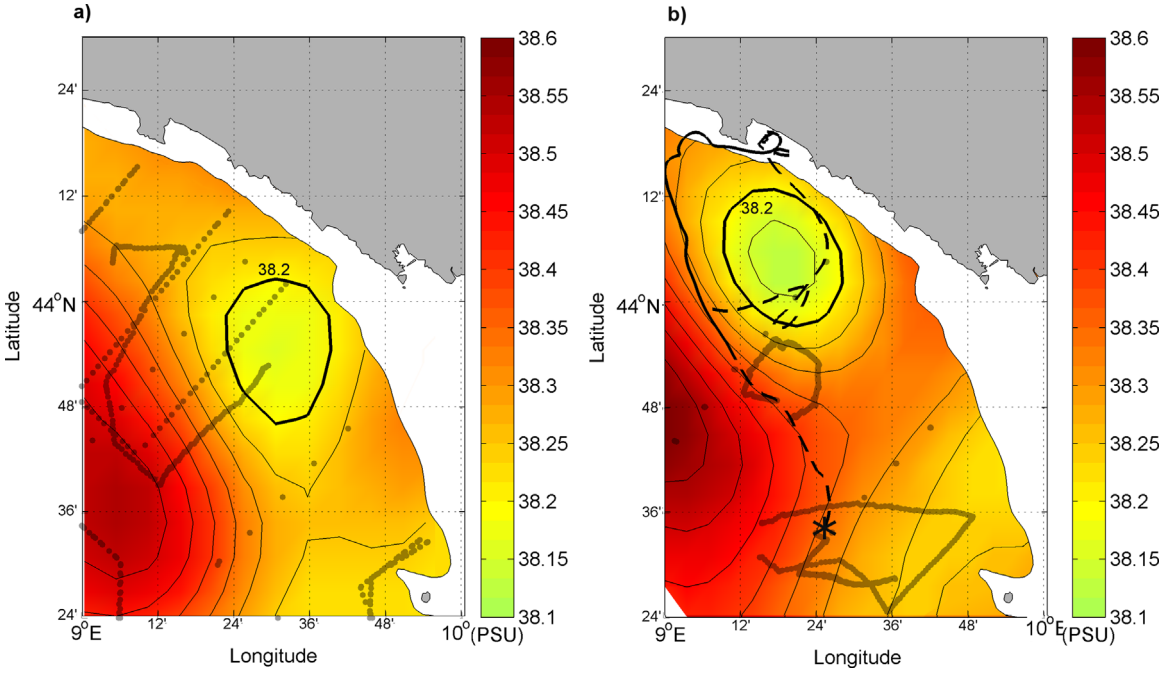

Fig. 11. Horizontal section of salinity at 150 m, as obtained from the interpolation of all salinity measurements obtained from CTD, ScanFish and glider profiles during 5–9 August (in panel a) and 16–20 August (in panel b). For reference, locations of the in situ observations used for the interpolation in each period are also marked. Salinity contours are drawn every 0.05 units to better characterize the salinity field in the region; the 38.2 salinity contour is drawn in bold. The trajectory followed between 2:48 (UTC) of 14 August and 8:58 (UTC) of 24 August by surface drifter ID n. 300234060607060 deployed during the cruise is also marked: a bold black line marks the drifter's trajectory that is contemporaneous to the salinity observations (i.e., between 16 and 20 August) while a dashed line marks its trajectory for periods prior to 16 August, and after 20 August 2013. The drifter deployment location at (9.42°E, 43.55°N) is marked by a star. Regions in white denote depths shallower than 150 m.

are small being mostly below 4 m day^{-1}. There are alternating bands of positive vertical velocities, which are indicative of upward transport, and bands of negative vertical velocities suggesting local downwards transport. Below 150 m, the intensity of vertical velocities increases slightly in magnitude yet remaining below 15 m day^{-1} and the alternation of upwards and downwards transport is more evident than near the surface. In the easternmost portion of the section the model-based estimates show a rather strong upwelling ($>$ 10 m day^{-1}) close to the continental shelf-break, in agreement with previous authors who showed similar patterns (Campbell et al., 2013; Casella et al., 2011). Conversely, such upwards transport in association to the coast is not as evident in the vertical velocities estimated through the Q vector formulation of the omega equation, where upward movement is limited to a smaller section close to the coast. The simulated fields only allow a snapshot in time of vertical velocities developing within the eddy, however it is possible that, similarly to the conclusions of Samuelsen et al. (2012), the alternating bands revolve within the eddy and change position and/or magnitude as the eddy moves northwestwards. Clearly, as long as direct

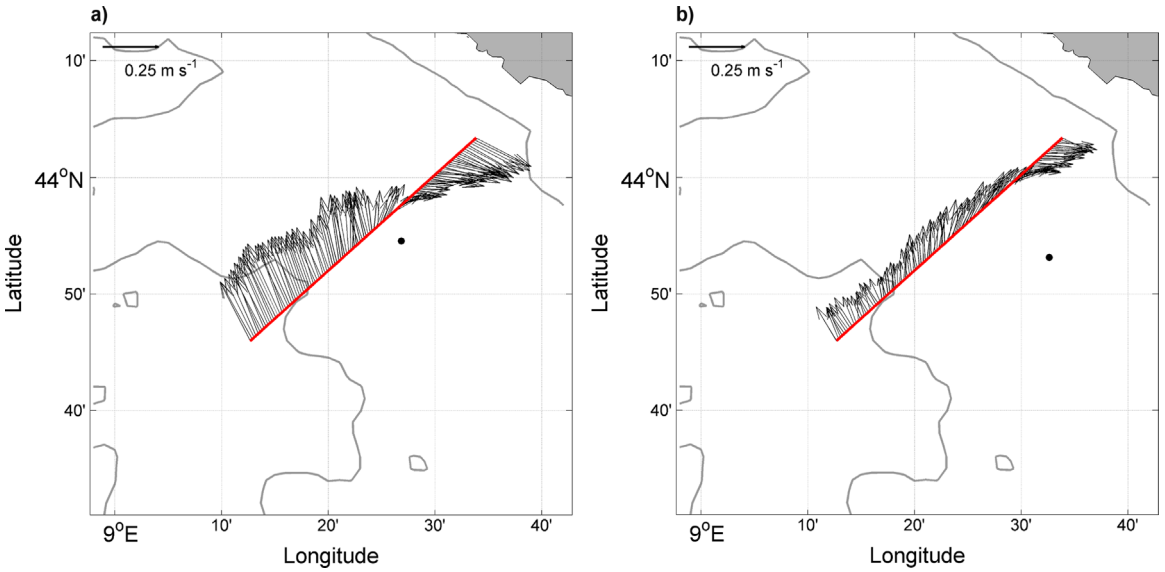

Fig. 12. ADCP currents measured at a) 30 m and b) 141 m depth during 7 August (00:04 AM–04:00 AM UTC). The red line denotes the ship transect for which current velocities were used to estimate the eddy centers. The eddy centers estimated from the direction of flow at the two depths are marked with a black dot. Thin grey lines denote bathymetry contours for the 200 m, 1000 m and 2000 m depth level. (For interpretation of the references to color in this figure legend, the reader is referred to the web version of this article.).

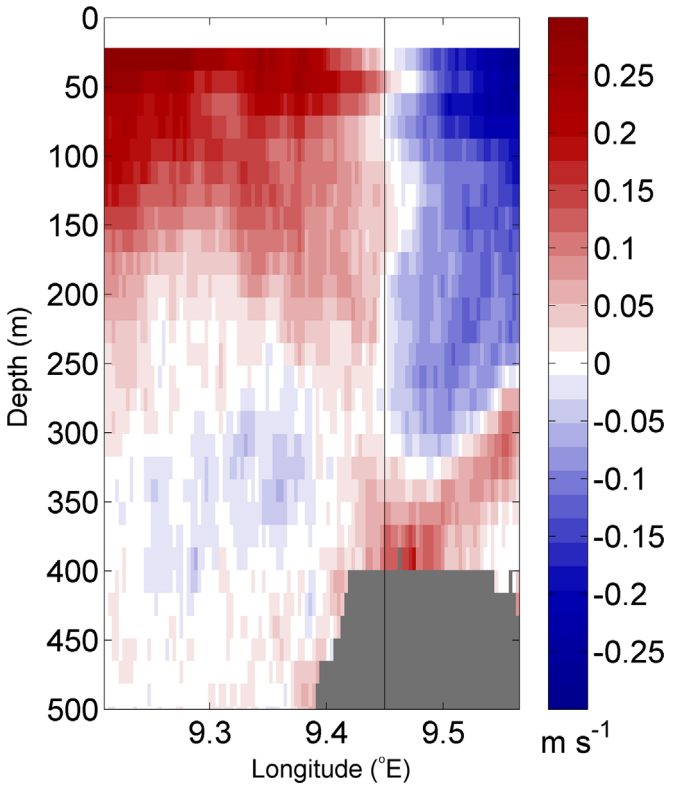

Fig. 13. Subsurface (≥ 30 m) magnitude of current velocities normal to the ship-borne ADCP transect during 7 August (marked in red in Fig. 12). For reference, the approximate location of the eddy center is marked with a vertical black line. Dark grey areas below 350 m denote measurements discarded because contaminated by the sea-floor. (For interpretation of the references to color in this figure legend, the reader is referred to the web version of this article.).

observations of the vertical velocities are not possible, the exact level of representativeness of the calculated vertical motions remains unknown (Buongiorno Nardelli et al., 2012; Samuelsen et al., 2012).

Vertical velocities obtained from model results and the Q vector formulation of the omega equation agree with the order of magnitude of vertical velocities derived from dimensional analysis (Cushman-Roisin, 1994), W=(Ro H U)/ L, where Ro stands for the Rossby number (i.e., 0.05), H represents the depth of the eddy (i.e., 350 m), U stands for the average horizontal velocity within the eddy (i.e., 0.2 m s^{-1}) and L approximates the horizontal length scale of the eddy (i.e., ~30 km). This calculation returns a value of ~10 m day^{-1} which is comparable to the modeled ones. The calculated Rossby number (0.05) is significantly smaller than unity and thus indicates that the eddy is in geostrophic balance (Cushman-Roisin, 1994).

Previous authors have shown that in the near-surface layers and just below the thermocline an anticyclonic recirculation is associated with low primary productivity levels, while a cyclonic recirculation is often associated with increased surface primary productivity (McGillicuddy and Robinson, 1997; Moutin and Prieur, 2012). The comparison between surface circulation and satellite-derived Chl *a* concentrations at the time of the in-situ observations (Fig. 15) confirms such correspondence for the Ligurian Sea. In fact, in the southeastern sector of the eddy, where the model estimates positive vertical velocities, Chl *a* concentrations are slightly higher than background values, while in the western sector of the eddy, where the model estimates negative vertical velocities, Chl *a* concentrations are at their minima and are equal or less than 0.1 mg m^{-3}. Conversely, the cyclonic circulation observed in the southwestern sector of the Ligurian sea is associated with higher Chl *a* concentrations ranging 0.15–0.2 mg m^{-3}. Indeed, as no in situ fluorescence measurements are available at the time of the cruise, it is currently not possible to verify if the particular patterns in Chl *a* concentrations are solely due to the vertical velocity patterns that develop within the observed anticyclonic eddy, or if other factors, such as input of nutrients through land runoff or wind activity may also play an important role in controlling the adjacent phytoplankton bloom (Borrione et al., 2014).

However, seeding (in offline mode) the model with passive floats along a section crossing the eddy center (Fig. 16) suggests that water particles located at least 15 km from its center (i.e., the potentially nutrient-rich coastal waters) cannot enter the eddy but are advected around it. The same trajectories indicate that NC water-particles to the west of the eddy are advected anticyclonically until they reach the coastal area, thus favoring a renewal of coastal shelf waters which are subsequently advected southward, exiting the model's domain. Only waters that are at less than 15 km from the eddy center will be captured by the anticyclonic flow that spirals towards the core of the eddy (i.e., the innermost blue trajectory), with a maximum period of 7 days. The period is here defined as the time required by a passive float to complete a full loop around the outermost periphery of the eddy core. This particular circulation scenario thus indicates that waters trapped within the core of the eddy are kept well separated from those located outside the eddy's attractor basin.

3.4. Eddy formation mechanism

One of the possible factors leading to the formation of an eddy is the presence of long-lasting intense winds (Hu et al., 2011; Piterbarg et al., 2014; Schaeffer et al., 2011). To verify the importance of the wind regime at the time of the MED-REP13 cruise, wind intensities between 01 July and 21 August 2013 (in Fig. 17) were extracted over the eddy area (rectangle in Fig. 19a) from the atmospheric model COSMO. Overall, daily wind velocities prior to the observation of the eddy remained below 5 m s^{-1} till the 9 of August, with few sporadic single-day peaks. Piterbarg et al. (2014) estimated that winds should blow at speeds of 10 m s^{-1} (i.e., ~20 kn) for at least 2.5-3 days to modify the 20 km wide and 200 m deep NC. Therefore, given the weak wind regime observed during the sea trial, we may exclude wind forcing as a mechanism leading to the formation of the observed anticyclonic eddy.

In the Ligurian Sea, the NC flows northwards north of Corsica along the 1000 m bathymetry contour (Figs. 1 and 8). Before turning west along the Italian-French coast, the NC reaches the shallower continental shelf region adjacent to La Spezia. One could expect that as the NC encounters shallower topography, to respect the law of conservation of potential vorticity, a decrease of layer thickness due to shallowing topography (i.e., squeezing) must be compensated by a decrease in relative vorticity (RV) (i.e., generation of negative vorticity) hence potentially leading to the formation of the observed anticyclonic eddy. This scenario may be verified with the calculation of the Burger number (Cushman-Roisin, 1994) which expresses the ratio of RV (~U/L; where U stands for the average horizontal velocity within the eddy and L approximates the horizontal length scale of the eddy) and vertical stretching (~f^2 U L/N^2 H^2; where f expresses the Coriolis parameter and N expresses the Brünt-Väisäla frequency). Based on a scale analysis, where U ~ 0.2 m s^{-1}; L~30 km; f ~ 10^{-5} m s^{-2}; N ~ 10^{-4} s^{-1}; H~350 m, the Burger number is large, i.e., ~1.4 10^4, indicating that the role vertical stretching/squeezing in relation to topographic variations is negligible compared to RV, which is four order of magnitudes higher.

When the mechanical-energy budget of the system is considered, the potential energy (PE) may be separated into the PE of

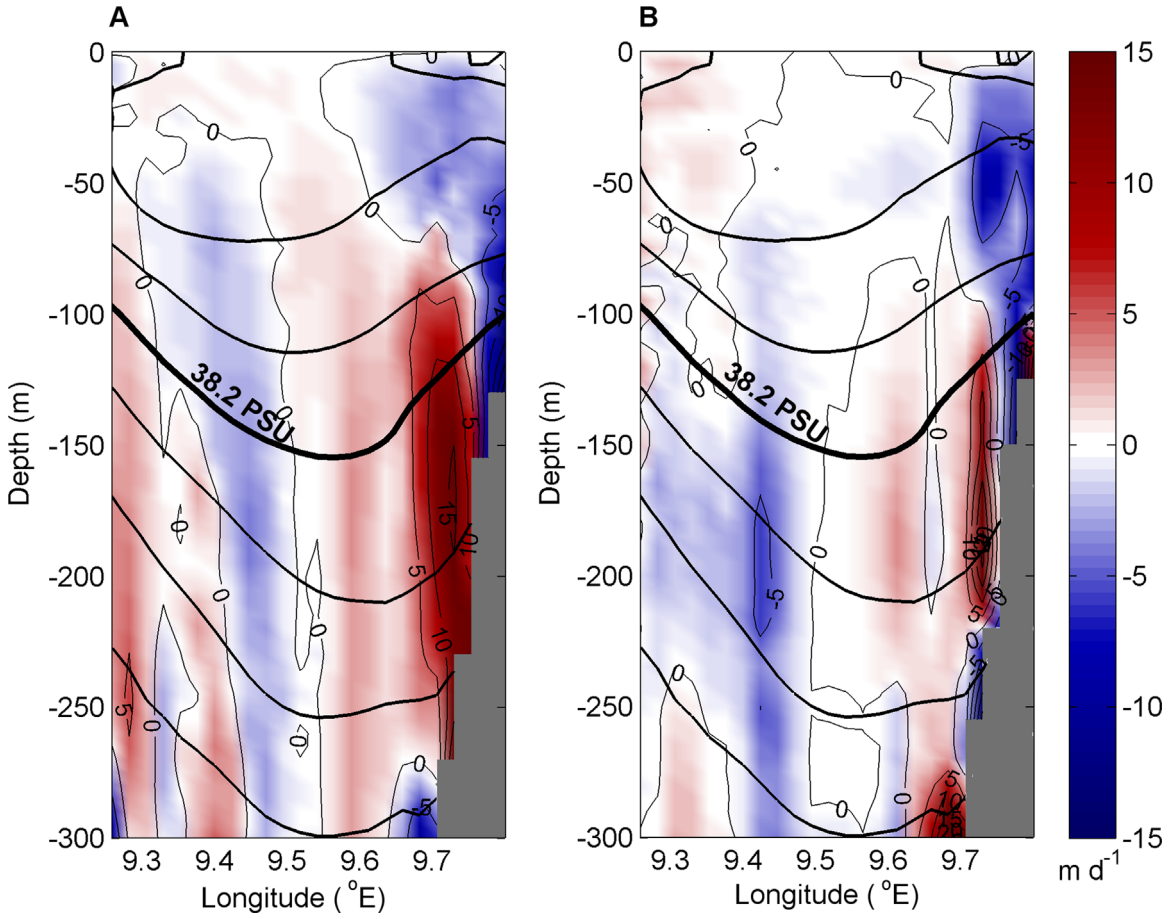

Fig. 14. Vertical velocities estimated from model results within the core of the eddy (9.25°E −9.8°E) and along the section defined along 43.87°N. Positive velocities are directed upwards. In a) velocities are obtained from model outputs, while in (b) they are obtained from the Q vector formulation of the omega equation applied to the model's temperature and salinity fields. As an indication of the eddy structure, we mark the isohalines also shown in Fig. 9b. Isohalines are marked every 0.2 PSU between 37.8 and 38.8; as reference, the 38.2 isohaline is marked with a bold line. Areas colored in dark grey denote the sea floor. (For interpretation of the references to color in this figure legend, the reader is referred to the web version of this article.)

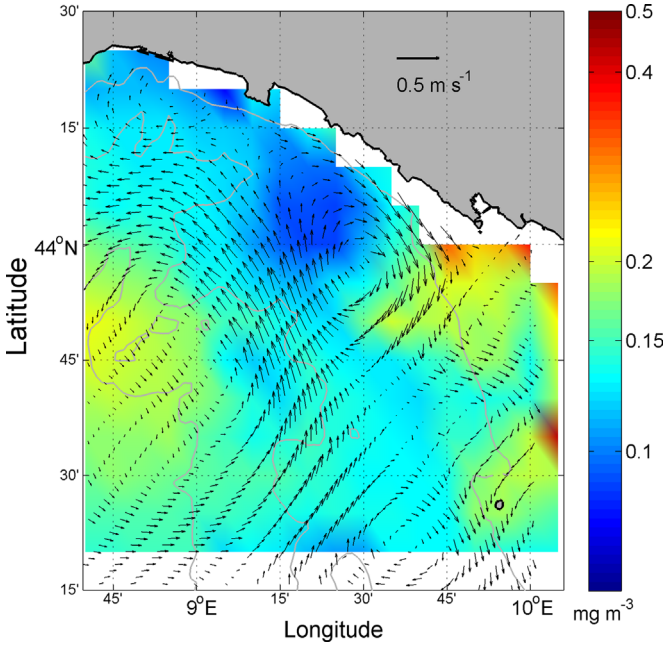

Fig. 15. Surface Chl *a* concentrations from 8 to 10 August (background color) and velocity fields (vectors) at 30 m depth as obtained from the stream function of ADCP measurements during 5–9 August. Bathymetry contours for the 200 m, 1000 m and 2000 m depth levels are marked with thin grey lines.

the mean field (i.e., the PE of an unperturbed state) and the PE available for conversion into kinetic energy (KE) via baroclinic instability (defined as APE), so that KE+(PE+APE)=0. In other words, the APE corresponds to the difference between the existing potential energy and the potential energy that the fluid would have if the basic stratification were unperturbed (Cushman-Roisin, 1994). In a state of geostrophic equilibrium APE is almost zero, and KE+PE=0. Fig. 18 shows the 0–300 m depth-averaged radial distribution of KE and APE calculated following their definition in Cushman-Roisin (1994) and using as reference the summer (July-September) climatological density profile obtained from all historic measurements extracted for the same area from the WOD13.

The variation of KE with distance from the eddy center (measured along a section due southwest) reflects the progressive increase of velocities in the region (see Fig. 6). At the center of the eddy, KE values are close to zero, and increase rapidly to values of $7.8*10^{11}$ J m^{-3} close to the limits of the eddy (~15 km radius). Farther away there is continuous, but more gradual, increase in KE which reflects the fact that the eddy is merged with the eastern side of the NC. Also the APE increases with distance from the eddy center, however it reaches its maximum values a bit before the edge of the eddy (~13 km), after which APE values remain rather constant, oscillating around $7*10^{7}$ J m^{-3}. Scale analysis between the two terms clearly shows that the KE is consistently four orders of magnitude larger than the APE. This is in clear agreement with Burger number obtained above (Cushman-Roisin, 1994) and indicates that baroclinic instability may not be responsible for eddy formation.

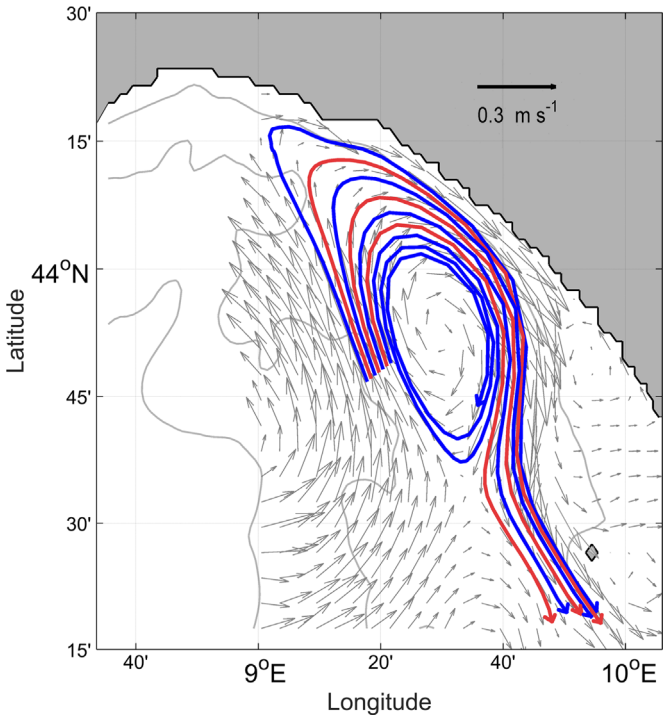

Fig. 16. Trajectories of 7 different passive floats seeded (in offline mode) in the model circulation along a transect crossing the center of the eddy.

Although the data collected during MED-REP13 does not cover the period of formation of the anticyclonic eddy, further research was conducted to hypothesize another possible mechanism responsible for its formation. In particular, drifter trajectories during MED-REP13 (Fig. 3) suggest a physical scenario in which the NC flows northwards and remains detached from the continental slope of the Northwestern Italian coast. The coastal boundary at the North constrains the jet to bifurcate into westward and eastward branches with associated cyclonic and anticyclonic circulations, respectively. This feature would suggest a relationship between the directionality of the NC when it leaves the area north of Corsica and enters the Ligurian Sea and favorable pre-conditions for anticyclonic eddy formation. Specifically, when the inflow of the NC is northward, adjustments between shear and orbital components of the RV (see Caniaux et al., 2001 or Cushman-Roisin, 1994) are possible in the marine region enclosed between the main current and the continental slope. Conversely, when the inflow of the NC is northeastward and adjusted to the continental slope the development of negative orbital vorticity in the eastern part of the jet is not possible. Satellite-derived surface geostrophic velocities from the 20-year period (January 1993 - December 2013) were used to investigate this possible relationship.

Altimetry-derived surface geostrophic currents were extracted along a 50 km transect crossing the mean location of the NC and over the northeastern sector of the Ligurian Sea to the right of the NC (regions marked respectively with a bold line and rectangle in Fig. 19a) to obtain the time-series of the direction and speed of the NC as it leaves the area north of Corsica and the time series of RV anomaly over the northeastern sector of the Ligurian Sea. The RV anomaly was derived with respect to the RV climatology, here calculated as the RV average over the chosen 20-year period (i.e., 1.9 10^{-6} m s^{-1}). For sake of clarity, the two time series shown in Fig. 19b and c pertain to the 2008–2013 period only.

Overall, both the direction of the NC and the RV anomaly exhibit large temporal variability. Based on this dataset, the average direction of the NC is due north-northeastwards (358°N −38°N), although the NC has flown more eastwards or more westwards than the average (example periods are marked with blue and green dots, respectively, in Fig. 19b).

Comparable temporal variability is observed in the time series of the RV anomaly, which on several occasions displays values that are significantly higher or lower than the average. In particular, periods of northeastwards flow of the NC (i.e., those marked with blue dots in Fig. 19b) are associated with positive peaks in the RV anomaly, while periods of northwestwards flow of the NC (i.e., those marked with green dots in Fig. 19b) are associated with negative peaks, suggesting a relationship between the directionality of the NC and the RV anomaly. The latter relationship becomes more evident in the scatter plot of RV anomaly values versus NC direction (Fig. 20a) where data for the whole 20-year period are used.

Overall, dots in the scatter plot relating the directionality of the NC to the RV anomaly (Fig. 20a) are aligned along a negatively sloped regression line that confirms the relationship between the two variables. Considering the 20-year timeseries it is possible to identify periods during which a north-northwestwards flow of the NC (i.e., a precondition for the formation of an anticyclonic eddy in the region, see Discussion section below) were associated to negative peaks in RV anomaly (i.e., colored dots in Fig. 20). Such relationship can be further confirmed by the correlation between the two variables which yields, in the 20-year long time series, a value of −0.6. Interestingly, observational evidences reported in the literature about the anticyclonic eddy (Alvarez et al., 2013; Schroeder et al., 2011) match with periods of anomalous negative values of RV and northward direction of the NC (vertical lines in Fig. 19b and c).

Conversely, there is no clear connection between the average speed of the NC and the RV anomaly. In fact, the scatter plot obtained from the two variables (Fig. 20b) defines a more or less circular area, with a more horizontal regression line and a correlation coefficient between the two time series is of −0.27. Consequently, the time series of the speed of the NC, and its relationship with RV anomaly is not analyzed further.

The sensitivity of the correlation coefficients and patterns described above to the size of the areas selected for the extraction of

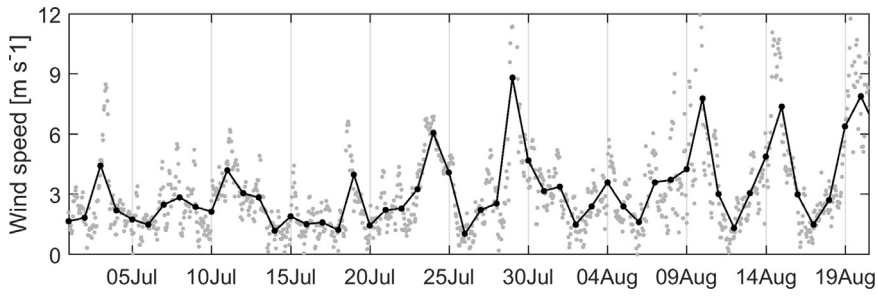

Fig. 17. Wind field over the eddy area (rectangle in Fig. 19a) as estimated from the atmospheric COSMO model. The black line and dots denote the 24-hr mean daily field, while grey dots denote hourly observations over the same area.

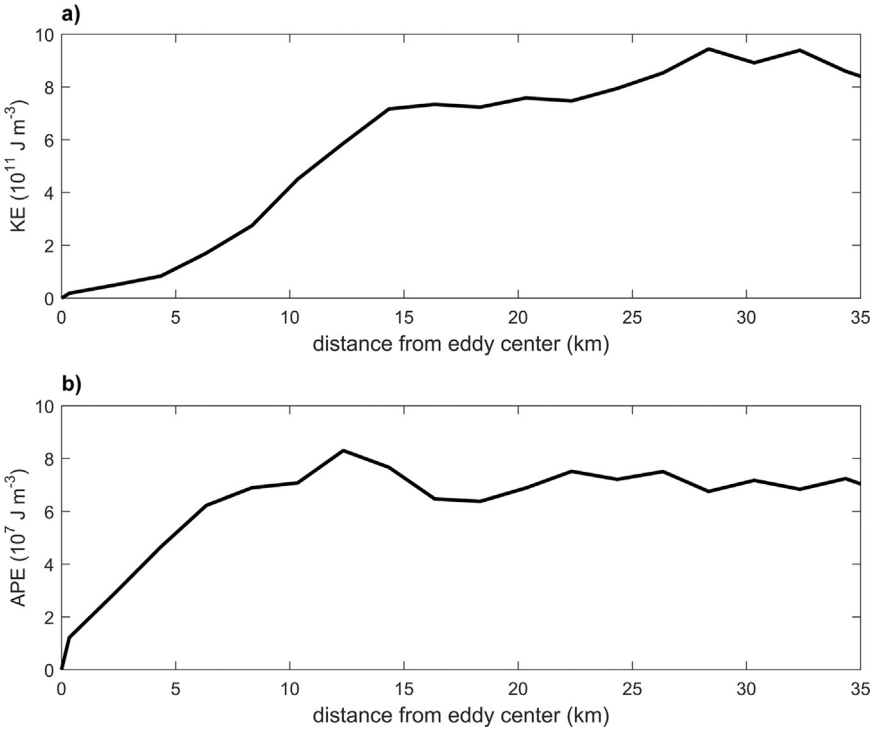

Fig. 18. Depth averaged a) kinetic energy (KE, units of 10^{11}) and b) available potential energy (APE, units of 10^{7}) calculated with increasing distance from the eddy center (9.5°E, 43.87°N). The two variables are calculated along a section due southwest of the eddy center.

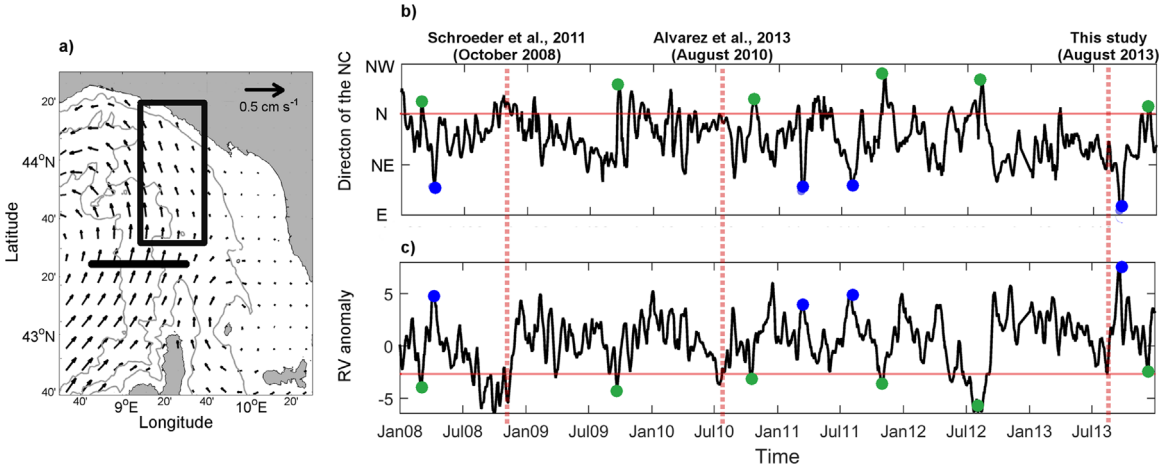

Fig. 19. a) Regions over which altimetry-derived surface geostrophic velocities were extracted to calculate the time series of the direction of the NC (black line) and the RV anomaly (rectangle). Vectors depict the 20-year (January 1993-December 2013) altimetry-derived average of surface geostrophic circulation. b) Time series of the direction of the NC calculated along the transect crossing the mean location of the NC (black line in panel a). For reference, the horizontal line denotes the Northwards direction; examples of periods during which the NC has flown more eastwards or westwards than the average are marked respectively with blue dots (i.e., around 03 April 2008, 09-Mar-2011, 03 August 2011, 23 September 2013) or green dots (i.e., around 29 February 2008, September-October 2008, 24 September 2009, 21 October 2010, 03 November 2011, 12 August 2012, 09 December 2013). **c**) Time series of RV anomaly (units are multiples of 10^{-6} m s^{-1}) calculated over the northeastern Ligurian Sea (rectangle in panel a). For reference, the horizontal line marks the RV anomaly calculated for August 2013. In panels b and c, vertical lines denote periods of anticyclonic recirculations documented in literature. (For interpretation of the references to color in this figure legend, the reader is referred to the web version of this article.).

the time series was tested, and returned comparable results in all cases. Also, correlations did not increase by adding a time lag in the calculations.

Periods during which the connection between north-north-westwards flow of the NC and anomalous negative RV values is more evident appear to recur with a near-annual frequency, mostly in the late summer-autumn months. Such recurrence was verified applying the Fast Fourier Transform (FFT) calculations to the 20-year long timeseries of RV anomaly. The FFT time-series analysis identifies in the data series the dominant periodic patterns that are permitted by the dataset's length and temporal interval, separating periodic oscillations from the random and aperiodic fluctuations (i.e., noise). The outcome of the Fourier analysis applied to the timeseries of RV anomaly (Fig. 21) confirms the anticipated near-annual frequency with a peak in power around periods of 374-358 days but also shows a pronounced peak at period of ~5 years and several peaks in power for periods shorter than 3 months (i.e., 2 and 1.5 months).

4. Discussion

The combined analysis of in situ measurements of temperature,

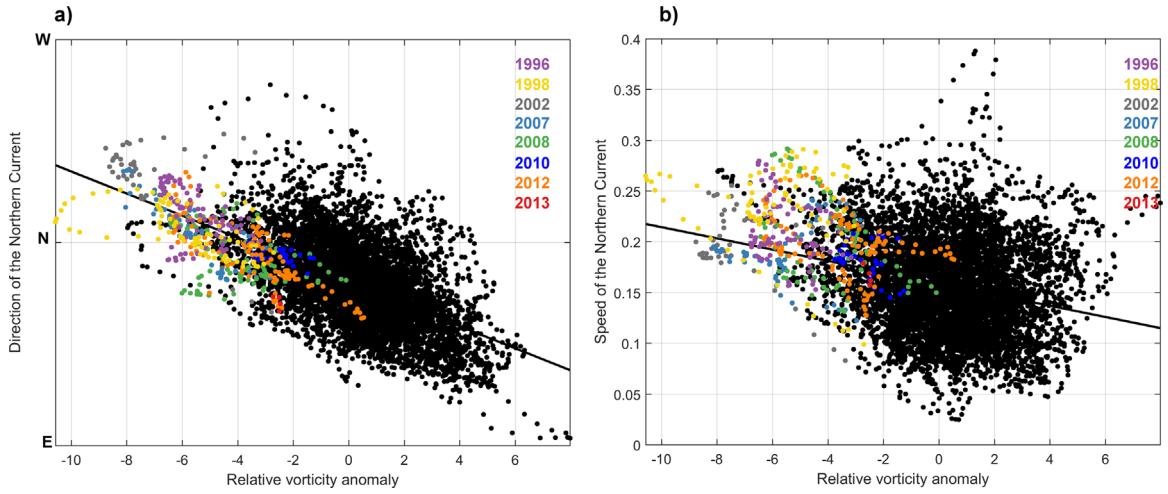

Fig. 20. Scatter plot of the direction (a) and speed (b) of the NC versus RV anomaly (units are multiples of 10^{-6} s^{-1}) from 1 January 1993–31 December 2013. The two quantities are calculated over the areas marked in Fig. 19a. Colored dots highlight periods during which the RV anomaly was comparable or more negative than the one calculated for August 2013 (horizontal line in Fig. 19c) and for which the link with the north-northwestwards flow of the NC is more evident. Colored dots are for July-October 1996; July–September 1998; August–October 2002; July–September 2007; July–October 2008; Aug 2010; May–September 2012; Aug 2013). The regression line between the two pairs of variables is also shown. (For interpretation of the references to color in this figure legend, the reader is referred to the web version of this article.).

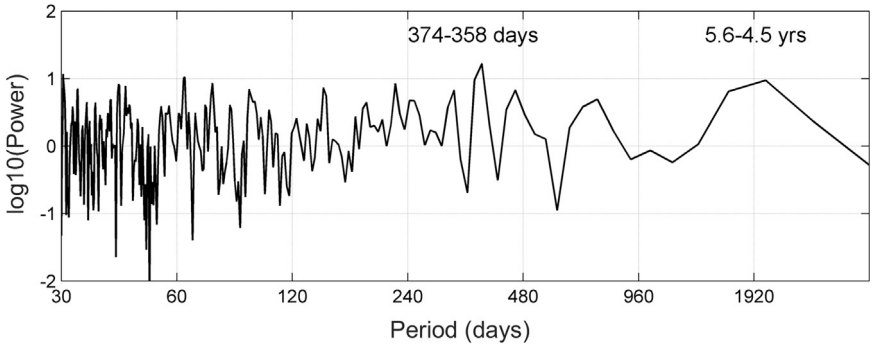

Fig. 21. Outcome of the FFT analysis applied to the timeseries of RV anomaly from 1993 to 2013.

Table 2
Main physical quantities of the observed eddy.

Physical quantity	Value
Average eddy radius	16 km
Rossby number	0.05
Burger number	1.3*10^4
Rossby radius of deformation (below the thermocline)	18.1 km
Position of eddy center	9.5°E; 43.96°N
Distance of eddy center from the coast	21 km
Maximum depth of the eddy	~320 m
Temperature and salinity at eddy mid depth (i.e., 150 m)	13.5 °C, 38.2 PSU
Maximum absolute vertical velocities at 150 m	15 m day^{-1}
Depth and magnitude of maximum horizontal velocities	45 m, 0.35 m s^{-1}
Estimated eddy translation speed	0.03 m s^{-1} (2.6 km day^{-1})

salinity and ocean currents acquired from different sampling platforms and model results has allowed a detailed characterization of an anticyclonic eddy observed between the inshore edge of the NC and the Ligurian coast around (9.5°E, 43.97°N). Its main characteristics are summarized in Table 2.

Some of the eddy characteristic summarized in Table 2 are comparable to those of other eddies described in the Northwest Mediterannean Sea. For example, the radius of the MED-REP13 eddy, is close to the 18–20 km range of radii estimated in the Gulf of Lions and the Catalan Sea (Flexas et al., 2002; Hu et al., 2011; Rubio et al., 2005), or in the Ligurian Sea by the modeling study of Casella et al. (2014). Although not measured directly, results shown in Schroeder et al. (2011) suggest a similar eddy size estimate. Comparable eddy sizes in all cases can be justified by the Rossby radius of deformation which in the northwest Mediterannean Sea ranges 10–20 km (Guihou et al., 2013; Marullo et al., 1985). Also the eddy trajectory and average drifting velocity resulting from our dataset agree well with those of the cyclonic and anticyclonic eddies simulated in other areas of the Northwest Mediterannean Sea (Hu et al., 2011; Rubio et al., 2009). The only information available for the Ligurian Sea derives from the results of Casella et al. (2011, 2014) who show that the majority of the Ligurian eddies found in their model outputs have formed and then drifted with speeds ranging 0.01–0.1 m s^{-1} along the path of the NC till the area offshore Genoa where they appear to fade out.

Conversely, when compared to previously observed or modeled eddies the depth of the MED-REP13 eddy (> 300 m) is significantly deeper causing it to occupy, at its center, most of the 500 m deep water column. In fact, the anticyclonic eddies identified in the Ligurian Sea with the model results of Casella et al. (2011) did not penetrate below 120 m, while the earlier in situ observations of Marullo et al. (1985) describe a superficial cyclonic eddy with depths ranging 50–100 m. Schroeder et al. (2011) identified an anticyclonic eddy offshore La Spezia during October 2008, however their study is based on surface drifters only so that nothing is known about the eddy's vertical structure, while the in situ measurements of Alvarez et al. (2013) partially captured a similar recirculation pattern, but did not sample the water column

below 160 m. Consequently the MED-REP13 eddy appears to be the deepest one observed to date in the northeastern sector of the Ligurian Sea; its proximity to the coast and vertical extent are likely to have important implications on the surrounding physical and biogeochemical environment, leading to an increased variability of the system. In fact, the TS diagrams obtained from the CTD casts (Fig. 4) show that during the first sampling period the area was mostly occupied by the fresher eddy waters, with salty MAW evidenced in the open-ocean casts of the northernmost CTD transect only. Conversely, 11 days later both CTD transects evidenced the presence of the saltier waters, indicating that as the eddy moved northwards, its previous position was progressively replenished by the saltier MAW.

A large scale effect of the MED-REP13 eddy is clearly evidenced by the horizontal velocity fields measured by the ADCP and reproduced by the model (Fig. 6). We could observe that along the northeastern coast of the Ligurian Sea at the time of the cruise surface circulation was directed southeastwards and not northwestwards as traditionally portrayed in the literature (i.e., Millot et al., 1999). These results confirm that similar eddies can lead to important modifications in the general circulation patterns, as previously shown by Pascual et al. (2002) in the Balearic Sea. Due to eddy presence in fact, the NC waters are advected anticyclonically around the eddy, causing a renewal of coastal waters. Moreover, as the eddy is located close to the coast, it will also favor cross-shelf mixing of coastal and open-ocean waters. This will lead to the exchange of heat and salt, but also the transport of macronutrients. The latter will have direct consequences on biogeochemistry considering that the Ligurian Sea is typically oligotrophic, and therefore any supply of nutrients is extremely important for the primary production (Campbell et al., 2013; Casella et al., 2014; Nezlin et al., 2004). Noteworthy is also the fact that this region of the Ligurian Sea is important for commercially valued marine species distributed around the shelf-break, whose nursery areas and dispersion depends also on the presence of recurrent oceanographic features such as fronts or eddies (Abella et al., 2008). The influence of an eddy on the surrounding environmental conditions can be extended over a large area if the eddy is not stationary, but translates away from the region where it has formed. Based on the size (i.e, 32-km diameter) and drifting speed (i.e., 0.03 m s^{-1} or $\sim$2.6 km day^{-1}) of the MED-REP13 eddy, we estimated that during the time of the cruise the eddy moved about 29 km northwards, thus influencing a surface area that is at least 700 km^2.

In the vertical dimension, the influence of an eddy on the characteristics of the water column is linked to its vertical velocities. In this study, vertical velocities were obtained from ROMS simulations, where the model was configured for a diagnostic run to reconstruct the velocity field that balanced observations (see Sect. 2.4). We found that vertical velocities exhibited the characteristic alignment in vertical bands of positive and negative vertical velocities described in previous observation-based and modeling studies (Buongiorno Nardelli et al., 2012; Koszalka et al., 2009; Viúdez and Dritschel, 2003). In the first 150 m absolute vertical velocities (i.e., 4 m day^{-1}) were smaller than those estimated by Casella et al. (2011) and Viúdez et al. (1996) (i.e., 17 and 15 m day^{-1}, respectively); nevertheless, they are still expected to modify regional temperature and salinity properties, as well as biogeochemistry (Campbell et al., 2013; Casella et al., 2011; Hu et al., 2011). Moreover, as shown in Fig. 9, isohaline and isotherm surfaces become deeper towards the center of the eddy, indicating a significantly deeper mixed layer depth than in surrounding waters. As a consequence, macronutrients and phytoplankton cells in the surface layer are diluted over a much larger volume, leading to a progressive reduction of primary productivity in the area influenced by the eddy. This effect is suggested by the ocean color image for 8-10 August depicted in Fig. 15. Considering all the physical and biogeochemical implications mentioned above, the recurrence of such eddy will clearly increase its relevance for the region.

In general, various dynamical processes can contribute to eddy formation (Albérola and Millot, 2003; McWilliams, 1985). Detachment of a coastal current from the coast when it encounters a sharp corner or a cape is one of the mechanisms for the formation of anti-cyclonic eddies proposed in the literature (Klinger, 1994; Pichevin and Nof, 1996). In the present case, however, there is no evident geographic feature with which the current may interact to justify the generation of the observed anti-cyclonic eddy. Moreover, a large Burger number indicates that for the REP13-eddy vertical squeezing due to topographic variations (shallowing) are negligible (Cushman-Roisin, 1994), in contrast with the formation mechanism of anticyclonic eddies in front of Marseille in the Gulf of Lions (Rubio et al., 2009). Other works have suggested that eddy formation may be linked to the wind stress curl generated by a strong and long lasting wind event (Casella et al., 2014; Hu et al., 2011; Pascual et al., 2002; Schaeffer et al., 2011) or in relation to a persistent fresh water input from river runoff (Schaeffer et al., 2011) which may modify stratification and vorticity. Daily wind intensities extracted over the eddy area for the period preceding our observations were weak, thus indicating that it is unlikely that the wind field may be connected to the formation of such deep structure, although it may be important in sustaining and fueling the eddy once it has formed (Hu et al., 2011). Moreover, the eddy path along the NC is too far from a significant riverine freshwater inflow for it to alter water properties down to the depth of the eddy.

Other possible mechanisms may be linked to the dynamical characteristics and variability of the NC, to which Casella et al. (2014) and Escudier et al. (2013) associate the highest values of eddy kinetic energy found in the whole LPB (see also Guihou et al., 2013). Several authors, for example, considered eddy-shedding due to the instability of the NC and its meandering nature (Crépon et al., 1982; Flexas et al., 2002; Marullo et al., 1985; Sammari et al., 1995). The presence of meanders along the path of the NC, clearly seen in satellite SST images, was explained by Crépon et al. (1982) and Sammari et al. (1995) using the two-layer model of Tang et al. (1975). Wind stress, variations in intensity of the current as well as topographic irregularities are the potential causes for the instability of a current (Flexas et al., 2005; Rubio et al., 2009; Wolfe et al., 2006). The very small APE values calculated within the REP13-eddy, however, would exclude a formation through baroclinic instability, although such explanation has been used for other eddies in the Ligurian sea such as the 6 km-radius cyclonic eddy described by Marullo et al. (1985) or the $<$120 m deep anticyclonic eddies described by Casella et al. (2014) and Flexas et al. (2002) in the Gulf of Lions, where baroclinic instability is viewed as a possible mechanism for the generation of NC meanders, and thus shedding of anticyclonic eddies along the coastal side of the NC current.

Altimetry maps were used to further investigate the possible formation mechanism of the anticyclonic eddy under study. Despite their very high resolution, altimetry tracks do not cover the observational area uniformly, while gridded altimetry products are too smooth to resolve small (order of 10–100 km) and coastal features (Amores et al., 2013; Escudier et al., 2013). Therefore efforts were aimed at linking the variability of general circulation features (extracted from the gridded altimetry fields) with conditions that are favorable to the generation of anti-cyclonic circulations in the MED-REP13 eddy area. Interestingly, results evidence the anti-correlation between the direction of the NC when it leaves the area north of Corsica and the appearance of significant negative anomalies of the large scale RV in the northeastern

Ligurian Sea. Specifically, pronounced negative anomalies in the region of interest are correlated with north-northwestwards orientations of the NC when it enters this marine area. Conversely, weak negative or even positive anomalies of RV are found when the NC enters the region with a northeastward orientation. In the case of north-northwestwards orientations of the NC, the current flows detached from the coast allowing adjustments in vorticity between the shear and orbital components of vorticity. This may force marginal fluid parcels with low vorticity and near the eastern edge of the NC, to separate from it and then recirculate to form an anti-cyclonic eddy to the right side of the NC (Cushman-Roisin, 1994). Drifter data (Fig. 3) clearly indicates that the NC jet bifurcates when it encounters the Italian coast. Interestingly, also Schroeder et al. (2011) documented that the anticyclonic eddy they observed with the trajectories of surface drifters released in October 2008 was located where the NC appeared to bifurcate. In the case of northeastward orientations of the NC, the current meets and flows along the continental slope thus preventing the vorticity adjustments discussed above. Changes in the inflow direction of the NC have been associated to its seasonal variability (Astraldi et al., 1990 ; Astraldi and Gasparini, 1992; Birol et al., 2010). These results, integrated with previous observations of anticyclonic eddies in the coastal area of the northeastern sector of the Ligurian Sea (Alvarez et al., 2013; Schroeder et al., 2011), suggest a link between the occurrence of anomalous negative RV values and the formation of anti-cyclonic eddies. Although Rubio et al., 2009 suggest that the intensification (and shear) of the NC, combined to the variation of topography encountered by the current as it approaches the Gulf of Lions may be responsible for the formation off Marseille, of the deep (>250 m) and low-density core anticyclonic eddies, we could not find a similar correspondence between pronounced negative anomalies in relative vorticity and the intensity of the NC.

To date the link between the directionality of the NC and the formation of similar anticyclonic eddies remains speculative but may give a preliminary indication that could be investigated by future research. If confirmed, the eddy may be a recurrent structure with a near-annual frequency mostly in the late summer-autumn months as it is suggested by the FFT analysis applied to the timeseries of RV anomaly.

5. Conclusions

During the MED-REP13 cruise in the northeastern sector of the Ligurian Sea an anticyclonic eddy was identified between the eastern edge of the NC and the Italian coast, over the continental shelf break. Using in situ observations from a variety of platforms, complemented by diagnostic simulations with ROMS, we could provide an unprecedented detailed characterization of the physical and dynamical features of this eddy. Similarly sized anticyclonic eddies are not new to the region, but they have never been observed to reach depths comparable to the one investigated here. Its anomalous penetration depth and position with respect to the NC indicates that, in contrast with previously investigate eddies, formation due to eddy-shedding from a meander of the NC most likely does not apply. Rather, the enforcement of the NC cyclonic flow and its northwards-northwestwards direction may be responsible for the eddy's formation. Results from this study not only contribute to a better understanding of the variability of circulation in the Ligurian Sea, which, as shown here, in some periods of the year can differ significantly from the circulation traditionally portrayed in the literature, but also integrates our current knowledge of the characteristics and formation dynamics of eddies in the same region. Finally, this study provides additional evidence of the advantages deriving from a networked ocean observing system where observations from very different in situ sampling platforms (among which autonomous platforms), satellite observations and modeling provide a unique picture of the environment, overcoming by far several of the limitations of each platform considered alone. This is an increasingly common approach to operational oceanography as it helps overcome the challenges of a spatially extended, highly variable and complex system like the ocean (Alvarez et al., 2013; Curtin and Bellingham, 2009).

Acknowledgements

We thank Richard Stoner, Marina Ampolo Rella, Gisella Baldasserini, Daniele Cecchi, Bartolomé Garau and Craig Lewis for their contribution to the deployments and recovery of gliders and drifters, as well as for the retrieval and processing of the data. We are also grateful to the officers and crew of the CMRE N/RV Alliance. We acknowledge Reiner Onken and Aniello Russo for constructive comments during the preparation of this manuscript. The four anonymous reviewers are also thanked for their constructive comments which greatly improved the quality of the manuscript. In this study, Taylor diagrams have been constructed using the MATLAB routines developed by Guillaume Maze (http://codes.guillaumemaze.org/taylor). The altimeter data were produced by Ssalto/Duacs and distributed by Aviso with support from CNES. This work has been partially funded by the Allied Command Transformation-ACT (NATO) (Project no. ACT000507) and the 7th Framework Programme (European Union) (FP7 2007–2013), under grant agreement no. 284321 (www.groom-fp7.eu).

Appendix A. Supporting information

Supplementary data associated with this article can be found in the online version at http://dx.doi.org/10.1016/j.dsr.2016.07.013.

References

Abella, A., Fiorentino, F., Mannini, A., Orsi Relini, L., 2008. Exploring relationships between recruitment of European hake (Merluccius merluccius L. 1758) and environmental factors in the Ligurian Sea and the Strait of Sicily (Central Mediterranean). J. Mar. Syst. 71, 279–293. http://dx.doi.org/10.1016/j.jmarsys.2007.05.010.

Albérola, C., Millot, C., 2003. Circulation in the French mediterranean coastal zone near Marseilles: the influence of wind and the Northern Current. Cont. Shelf Res. 23, 587–610. http://dx.doi.org/10.1016/S0278-4343(03)00002-5.

Albérola, C., Millot, C., Font, J., 1995. On the seasonal and mesoscale variabilities of the Northern Current during the PRIMO-0 experiment in the western Mediterranean-sea. Oceanol. Acta 18, 163–192.

Allou, A., Forget, P., Devenon, J.L., 2010. Submesoscale vortex structures at the entrance of the Gulf of Lions in the Northwestern Mediterranean Sea. Cont. Shelf Res. 30, 724–732. http://dx.doi.org/10.1016/j.csr.2010.01.006.

Alvarez, a, Chiggiato, J., Schroeder, K., 2013. Mapping sub-surface geostrophic currents from altimetry and a fleet of gliders. Deep Res. Part I Oceanogr. Res. Pap. 74, 115–129. http://dx.doi.org/10.1016/j.dsr.2012.10.014.

Alvarez, A., Mourre, B., 2012. Oceanographic field estimates from remote sensing and glider fleets. J. Atmos. Ocean. Technol. 29, 1657–1662. http://dx.doi.org/10.1175/JTECH-D-12-00015.1.

Amores, A., Monserrat, S., Marcos, M., 2013. Vertical structure and temporal evolution of an anticyclonic eddy in the Balearic Sea (western Mediterranean). J. Geophys. Res. Ocean 118, 2097–2106. http://dx.doi.org/10.1002/jgrc.20150.

Astraldi, M., Gasparini, G.P., 1992. The seasonal characteristics of the circulation in the north Mediterranean basin and their relationship with the atmospheric-climatic conditions. J. Geophys. Res. 97, 9531. http://dx.doi.org/10.1029/92JC00114.

Astraldi, M., Gasparini, G.P., Manzella, G.M.R., Hopkins, T.S., 1990. Temporal variability of currents in the eastern Ligurian Sea. J. Geophys. Res. 95, 1515. http://dx.doi.org/10.1029/JC095iC02p01515.

Baldauf, M., Seifert, A., Forstner, J., Majewski, D., Raschendorfer, M., Reinhardt, T., 2011. Operational convective-scale numerical weather prediction with the COSMO model: description and sensitivities. Mon. Weather Rev. 139,

3887–3905.
Birol, F., Cancet, M., Estournel, C., 2010. Aspects of the seasonal variability of the Northern current (NW Mediterranean Sea) observed by altimetry. J. Mar. Syst. 81, 297–311. http://dx.doi.org/10.1016/j.jmarsys.2010.01.005.
Blumberg, A.F., Mellor, G.L., 1983. Diagnostic and prognostic numerical circulation studies of the South Atlantic Bight. J. Geophys. Res. 88, 4579. http://dx.doi.org/10.1029/JC088iC08p04579.
Borrione, I., Aumont, O., Nielsdóttir, M.C., Schlitzer, R., 2014. Sedimentary and atmospheric sources of iron around South Georgia, Southern Ocean: a modelling perspective. Biogeosciences 11, 1981–2001. http://dx.doi.org/10.5194/bg-11-1981–2014.
Boyer, T.P., Antonov, J.I., Baranova, O.K., Coleman, C., Garcia, H.E., Grodsky, A., Johnson, D.R., Locarnini, R.A., Mishonov, A.V., O'Brien, T.D., Paver, C.R., Reagan, J. R., Seidov, D., Smolyar, I.V., Zweng, M.M., 2013. World Ocean Database 2013, NOAA Atlas NESDIS 72. In: Levitus, S. (Ed.), A. Mishonov, Technical. Silver Spring, MD, p. 209. http://dx.doi.org/10.7289/V5NZ85MT.
Buongiorno Nardelli, B., Guinehut, S., Pascual, A., Drillet, Y., Ruiz, S., Mulet, S., 2012. Towards high resolution mapping of 3-D mesoscale dynamics from observations. Ocean Sci. 8, 885–901. http://dx.doi.org/10.5194/os-8-885-2012.
Campbell, R., Diaz, F., Hu, Z., Doglioli, A., Petrenko, A., Dekeyser, I., 2013. Nutrients and plankton spatial distributions induced by a coastal eddy in the Gulf of Lion. Insights from a numerical model. Prog. Oceanogr. 109, 47–69. http://dx.doi.org/10.1016/j.pocean.2012.09.005.
Caniaux, G., Prieur, L., Giordani, H., Hernandez, F., Eymard, L., 2001. Observation of the circulation in the newfoundland basin in winter 1997. J. Phys. Oceanogr. 31, 689–710. http://dx.doi.org/10.1175/1520–0485(2001)031 < 0689:OOTCIT > 2.0.CO;2.
Casella, E., Molcard, A., Provenzale, A., 2011. Mesoscale vortices in the Ligurian Sea and their effect on coastal upwelling processes. J. Mar. Syst. 88, 12–19. http://dx.doi.org/10.1016/j.jmarsys.2011.02.019.
Casella, E., Tepsich, P., Coulevard, X., Caldeira, R.M.A., Schroeder, K., 2014. Ecosystem dynamics in the Liguro-Provençal Basin: the role of eddies in the biological production. Mediterr. Mar. Sci. . http://dx.doi.org/10.12681/mms.520
Chu, P.C., Fang, C.-L., Kim, C.S., 2005. Japan/East Sea model predictability. Cont. Shelf Res. 25, 2107–2121. http://dx.doi.org/10.1016/j.csr.2005.03.006.
Conan, P., Millot, C., 1995. Variability of the northern current off Marseilles, Western Mediterranean Sea, from February to June 1992. Oceanol. Acta 18, 193–205.
Crépon, M., Wald, L., Monget, J.M., 1982. Low-frequency waves in the Ligurian Sea during December 1977. J. Geophys. Res. 87, 595. http://dx.doi.org/10.1029/JC087iC01p00595.
Curtin, T.B., Bellingham, J.G., 2009. Progress toward autonomous ocean sampling networks. Deep Sea Res. Part II Top. Stud. Oceanogr. 56, 62–67. http://dx.doi.org/10.1016/j.dsr2.2008.09.005.
Cushman-Roisin, B., 1994. Introduction to Geophysical Fluid Dynamics. Prentice-Hall International, UK.
Dong, C., Lin, X., Liu, Y., Nencioli, F., Chao, Y., Guan, Y., Chen, D., Dickey, T., McWilliams, J.C., 2012. Three-dimensional oceanic eddy analysis in the Southern California Bight from a numerical product. J. Geophys. Res. Ocean 117, 1–17. http://dx.doi.org/10.1029/2011JC007354.
Echevin, V., Crépon, M., Mortier, L., 2003. Simulation and analysis of the mesoscale circulation in the northwestern Mediterranean Sea. Ann. Geophys. 21, 281–297. http://dx.doi.org/10.5194/angeo-21-281-2003.
Escudier, R., Bouffard, J., Pascual, A., Poulain, P.-M., Pujol, M.-I., 2013. Improvement of coastal and mesoscale observation from space: application to the Northwestern Mediterranean Sea. Geophys. Res. Lett. 40, 2148–2153. http://dx.doi.org/10.1002/grl.50324.
Flexas, M.M., Durrieu de Madron, X., Garcia, M. a, Canals, M., Arnau, P., 2002. Flow variability in the Gulf of Lions during the MATER HFF experiment (March–May 1997). J. Mar. Syst. 33–34, 197–214. http://dx.doi.org/10.1016/S0924-7963(02)00059-3.
Flexas, M.M., van Heijst, G.J.F., Trieling, R.R., 2005. The behavior of jet currents over a continental slope topography with a possible application to the northern current. J. Phys. Oceanogr. 35, 790–810. http://dx.doi.org/10.1175/JPO2705.1.
Garau, B., Alvarez, A., Oliver, G., 2006. AUV Navigation through turbulent ocean environments supported by onboard H-ADCP. In: Proceedings of the IEEE Int. Conf. Robot. Autom. 2006, 3556–3561. doi:10.1109/ROBOT.2006.1642245.
Guihou, K., Marmain, J., Ourmières, Y., Molcard, A., Zakardjian, B., Forget, P., 2013. A case study of the mesoscale dynamics in the North-Western Mediterranean Sea: a combined data–model approach. Ocean Dyn. 63, 793–808. http://dx.doi.org/10.1007/s10236-013-0619-z.
Hu, Z.Y., Petrenko, A.A., Doglioli, a M., Dekeyser, I., 2011. Study of a mesoscale anticyclonic eddy in the western part of the Gulf of Lion. J. Mar. Syst. 88, 3–11. http://dx.doi.org/10.1016/j.jmarsys.2011.02.008.
Kersalé, M., Petrenko, A.A., Doglioli, a M., Dekeyser, I., Nencioli, F., 2013. Physical characteristics and dynamics of the coastal Latex09 eddy derived from in situ data and numerical modeling. J. Geophys. Res. Ocean 118, 399–409. http://dx.doi.org/10.1029/2012JC008229.
Klinger, B.A., 1994. Baroclinic eddy generation at a sharp corner in a rotating system. J. Geophys. Res. 99, 12515. http://dx.doi.org/10.1029/93JC03585.
Koszalka, I., Bracco, A., McWilliams, J.C., Provenzale, A., 2009. Dynamics of wind-forced coherent anticyclones in the open ocean. J. Geophys. Res. 114, C08011. http://dx.doi.org/10.1029/2009JC005388.
Large, W.G., Gent, P.R., 1999. Validation of vertical mixing in an equatorial ocean model using large eddy simulations and observations. J. Phys. Oceanogr. 29, 449–464. http://dx.doi.org/10.1175/1520-0485(1999)029 < 0449:VOVMIA > 2.0.CO;2.
Li, Z., Chao, Y., McWilliams, J.C., Ide, K., 2008. A three-dimensional variational data assimilation scheme for the regional Ocean modeling system: implementation and basic experiments. J. Geophys. Res. 113, C05002. http://dx.doi.org/10.1029/2006JC004042.
Marchesiello, P., McWilliams, J.C., Shchepetkin, A., 2001. Open boundary conditions for long-term integration of regional oceanic models. Ocean Model. 3, 1–20. http://dx.doi.org/10.1016/S1463-5003(00)00013-5.
Marullo, S., Salusti, E., Viola, A., 1985. Observations of a small-scale baroclinic eddy in the Ligurian Sea. Deep Sea Res. Part A. Oceanogr. Res. Pap. 32, 215–222. http://dx.doi.org/10.1016/0198–0149(85)90029-9.
McGillicuddy, D.J., Robinson, A.R., 1997. Eddy-induced nutrient supply and new production in the Sargasso Sea. Deep Sea Res. Part I Oceanogr. Res. Pap. 44, 1427–1450. http://dx.doi.org/10.1016/S0967-0637(97)00024-1.
McWilliams, J.C., 1985. Submesoscale, coherent vortices in the ocean. Rev. Geophys. 23, 165. http://dx.doi.org/10.1029/RG023i002p00165.
Millot, C., 1987. Circulation in the Western Mediterranean Sea. Oceanol. Acta 10, 143–149.
Millot, C., 1991. Mesoscale and seasonal variabilities of the circulation in the western Mediterranean. Dyn. Atmos. Ocean. 15, 179–214. http://dx.doi.org/10.1016/0377–0265(91)90020-G.
Millot, C., 1999. Circulation in the Western Mediterranean Sea. J. Mar. Syst. 20, 423–442. http://dx.doi.org/10.1016/S0924-7963(98)00078-5.
Moore, A.M., Arango, H.G., Di Lorenzo, E., Miller, A.J., Cornuelle, B.D., 2009. An adjoint sensitivity analysis of the Southern California current circulation and ecosystem. J. Phys. Oceanogr. 39, 702–720. http://dx.doi.org/10.1175/2008JPO3740.1.
Moutin, T., Prieur, L., 2012. Influence of anticyclonic eddies on the Biogeochemistry from the Oligotrophic to the Ultraoligotrophic Mediterranean (BOUM cruise). Biogeosciences 9, 3827–3855. http://dx.doi.org/10.5194/bg-9-3827–2012.
Nezlin, N.P., 2004. Remotely sensed seasonal dynamics of phytoplankton in the Ligurian Sea in 1997–1999. J. Geophys. Res. 109, 1–12. http://dx.doi.org/10.1029/2000JC000628.
Pascual, A., Nardelli, B.B., Larnicol, G., Emelianov, M., Gomis, D., 2002. A case of an intense anticyclonic eddy in the Balearic Sea (Western Mediterranean). J. Geophys. Res. 107, 3183. http://dx.doi.org/10.1029/2001JC000913.
Petrenko, A.A., 2003. Variability of circulation features in the Gulf of Lion NW Mediterranean Sea. Importance of inertial currents. Oceanol. Acta 26, 323–338. http://dx.doi.org/10.1016/S0399-1784(03)00038-0.
Pichevin, T., Nof, D., 1996. The eddy cannon. Deep Sea Res. Part I Oceanogr. Res. Pap. 43, 1475–1507. http://dx.doi.org/10.1016/S0967-0637(96)00064-7.
Piterbarg, L., Taillandier, V., Griffa, A., 2014. Investigating frontal variability from repeated glider transects in the Ligurian Current (North West Mediterranean Sea). J. Mar. Syst. 129, 381–395. http://dx.doi.org/10.1016/j.jmarsys.2013.08.003.
Poulain, P.-M., Gerin, R., Mauri, E., Pennel, R., 2009. Wind effects on drogued and undrogued drifters in the Eastern Mediterranean. J. Atmos. Ocean. Technol. 26, 1144–1156. http://dx.doi.org/10.1175/2008JTECHO618.1.
Poulain, P.M., Gerin, R., Rixen, M., Zanasca, P., Teixeira, J., Griffa, A., Molcard, A., de Marte, M., Pinardi, N., 2012. Aspects of the surface circulation in the Liguro-Provençal basin and Gulf of Lion as observed by satellite-tracked drifters (2007–2009). Boll. Geofis. Teor. Appl. 53, 261–279. http://dx.doi.org/10.4430/bgta0052.
Rubio, A., Arnau, P. a, Espino, M., Flexas, Del Mar, Jordà, M., Salat, G., Puigdefàbregas, J., Arcilla, A.S, J., 2005. A field study of the behaviour of an anticyclonic eddy on the Catalan continental shelf (NW Mediterranean). Prog. Oceanogr. 66, 142–156. http://dx.doi.org/10.1016/j.pocean.2004.07.012.
Rubio, A., Barnier, B., Jordà, G., Espino, M., Marsaleix, P., 2009. Origin and dynamics of mesoscale eddies in the Catalan Sea (NW Mediterranean): insight from a numerical model study. J. Geophys. Res. Ocean 114, 1–17. http://dx.doi.org/10.1029/2007JC004245.
Ruiz, S., Pascual, A., Garau, B., Faugère, Y., Alvarez, A., Tintoré, J., 2009. Mesoscale dynamics of the Balearic Front, integrating glider, ship and satellite data. J. Mar. Syst. 78, S3–S16. http://dx.doi.org/10.1016/j.jmarsys.2009.01.007.
Russo, A., Coluccelli, A., Iermanno, I., Falcieri, F., Ravaioli, M., Bortoluzzi, G., Focaccia, P., Stanghellini, G., Ferrari, C.R., Chiggiato, J., Deserti, M., 2009. An operational system for forecasting hypoxic events in the northern Adriatic Sea. Geofizika 26, 191–213.
Sammari, C., Millot, C., Prieur, L., 1995. Aspects of the seasonal and mesoscale variabilities of the Northern Current in the western Mediterranean Sea inferred from the PROLIG-2 and PROS-6 experiments. Deep Sea Res. Part I Oceanogr. Res. Pap. 42, 893–917. http://dx.doi.org/10.1016/0967-0637(95)00031-Z.
Samuelsen, A., Hjøllo, S.S., Johannessen, J.A., Patel, R., 2012. Particle aggregation at the edges of anticyclonic eddies and implications for distribution of biomass. Ocean Sci. 8, 389–400. http://dx.doi.org/10.5194/os-8-389-2012.
Schaeffer, A., Molcard, A., Forget, P., Fraunié, P., Garreau, P., 2011. Generation mechanisms for mesoscale eddies in the Gulf of Lions: Radar observation and modeling. Ocean Dyn. 61, 1587–1609. http://dx.doi.org/10.1007/s10236-011-0482-8.
Schroeder, K., Haza, A.C., Griffa, A., Özgökmen, T.M., Poulain, P.M., Gerin, R., Peggion, G., Rixen, M., 2011. Relative dispersion in the Liguro-Provençal basin: from submesoscale to mesoscale. Deep. Res. Part I Oceanogr. Res. Pap. 58, 209–228. http://dx.doi.org/10.1016/j.dsr.2010.11.004.
Schroeder, K., Taillandier, V., Vetrano, a, Gasparini, G.P., 2008. The circulation of the western Mediterranean Sea in spring 2005 as inferred from observations and from model outputs. Deep-Sea Res. Part I Oceanogr. Res. Pap. 55, 947–965. http://dx.doi.org/10.1016/j.dsr.2008.04.003.
Shchepetkin, A.F., McWilliams, J.C., 2005. The regional oceanic modeling system (ROMS): a split-explicit, free-surface, topography-following-coordinate oceanic model. Ocean Model. 9, 347–404. http://dx.doi.org/10.1016/j.ocemod.2004.08.002.

Shearman, R.K., Barth, J.A., Allen, J.S., Haney, R.L., 2000. Diagnosis of the three-dimensional circulation in mesoscale features with large rossby number. J. Phys. Oceanogr. 30, 2687–2709. http://dx.doi.org/10.1175/1520-0485(2001)031 < 2687:DOTTDC > 2.0.CO;2.

Smith, W.H., Sandwell, D.T., 1997. Global Sea Floor Topography from Satellite Altimetry and Ship Depth Soundings. Science 277, 1956–1962. http://dx.doi.org/10.1126/science.277.5334.1956.

Taillandier, V., Griffa, a, Poulain, P.M., Béranger, K., 2006. Assimilation of Argo float positions in the North Western Mediterranean Sea and impact on ocean circulation simulations. Geophys. Res. Lett. 33, 1–5. http://dx.doi.org/10.1029/2005GL025552.

Tang, C.-M., 1975. Baroclinic instability of stratified shear flows in the ocean and atmosphere. J. Geophys. Res. 80, 1168–1175. http://dx.doi.org/10.1029/JC080i009p01168.

Taupier-Letage, I., Millot, C., 1986. General hydrodynamical features in the Ligurian Sea inferred from the Dyomé experiment. Oceanol. Acta 9, 119–131.

Taylor, K.E., 2001. Summarizing multiple aspects of model performance in a Single Diagram. J. Geophys. Res. 106, 7183–7192. http://dx.doi.org/10.1029/2000JD900719.

Tintoré, J., Wang, D.-P., La Violette, P.E., 1990. Eddies and thermohaline intrusions of the shelf/slope front off the northeast Spanish coast. J. Geophys. Res. 95, 1627. http://dx.doi.org/10.1029/JC095iC02p01627.

Umlauf, L., Burchard, H., 2003. A generic length-scale equation for geophysical turbulence models. J. Mar. Res. 61, 235–265. http://dx.doi.org/10.1357/002224003322005087.

Viúdez, Á., Dritschel, D.G., 2003. Vertical velocity in mesoscale geophysical flows. J. Fluid Mech. 483, 199–223. http://dx.doi.org/10.1017/S0022112003004191.

Viúdez, Á., Tintoré, J., Haney, R.L., 1996. Circulation in the Alboran Sea as determined by quasi-synoptic hydrographic observations. part i: three-dimensional structure of the two anticyclonic gyres. J. Phys. Oceanogr. 26, 684–705. http://dx.doi.org/10.1175/1520–0485(1996)026 < 0684:CITASA > 2.0.CO;2.

Wolfe, C.L., Cenedese, C., 2006. Laboratory experiments on eddy generation by a buoyant coastal current flowing over variable bathymetry*. J. Phys. Oceanogr. 36, 395–411. http://dx.doi.org/10.1175/JPO2857.1.

Zavatarelli, M., 2002. Diagnostic and prognostic model studies of the Adriatic Sea general circulation: seasonal variability. J. Geophys. Res. 107, 3004. http://dx.doi.org/10.1029/2000JC000210.

Document Data Sheet

Security Classification		Project No.
Document Serial No.	**Date of Issue**	**Total Pages**
CMRE-PR-2019-072	June 2019	20 pp.

Author(s)

Ines Borrione, Silvia Falchetti, Alberto Alvarez

Title

Physical and dynamical characteristics of a 300 m-deep anticyclonic eddy in the Ligurian Sea (Northwest Mediterranean Sea): evidence from a multi-platform sampling strategy

Abstract

We describe the physical and dynamical characteristics of a mesoscale anticyclonic eddy observed in August 2013 over the shelf-break region of the northeastern sector of the Ligurian Sea, between the northeastern edge of the Northern Current (NC) and the coast. Results derive from a dense dataset of temperature, salinity and current measurements obtained from a multi-platform sampling strategy as well as from a diagnostic simulation with the Regional Ocean Modeling System (ROMS) at a horizontal resolution of 1.8 km. Model results are obtained from a strong nudging to observations and, as they are physically balanced, they allow a three-dimensional diagnosis of the dynamics and physical characteristics of the eddy. The eddy is centred around 9.5°E, 43.94°N, about 20 km from the coast, and has a radius of 16 km. It is characterized by low-density waters and penetrates the thermocline down to at least 300 m reflecting the main features of the NC. Horizontal velocities near the surface are around0.4 m s 1, while at 150 m are still significantly high and close to 0.2 m s 1. Vertical velocities were estimated from model results; absolute values are below 4 m day 1until depths shallower than 150 m and increase with depth to 15 m day 1. The eddy's presence inverts the northwestwards flow traditionally portrayed in the region determining a southeastwards coastal circulation that replenishes coastal waters with those originating from the NC. We discuss several possible eddy formation mechanisms and suggest that its formation depends on the directionality of the NC when it enters the Ligurian Sea, as a result of the adjustment of the shear and orbital components of the current's relative vorticity.

Keywords

Ligurian Sea, Mesoscale circulation, Anticyclonic eddy, Regional Ocean Modelling System, Gliders

Issuing Organization

NATO Science and Technology Organization
Centre for Maritime Research and Experimentation

Viale San Bartolomeo 400, 19126 La Spezia, Italy

[From N. America:
STO CMRE
Unit 31318, Box 19, APO AE 09613-1318]

Tel: +39 0187 527 361
Fax:+39 0187 527 700

E-mail: library@cmre.nato.int